DD

UR-1371/ER40685-821

Quality Control Studies of Scintillating Tile/Fiber Megatile Production for the CDF End Plug Upgrade Hadron Calorimeter

P.de Barbaro, K. Michaud, A. Bodek, H. S. Budd,
Q. Fan, M. Olsson, M. Pillai and W. K. Sakumoto
University of Rochester

M. Albrow, R. Bossert, S. Delchamps, K. Ewald, J. Freeman, J. Kerby,
W. Koska, P.J. Limon, F. Nobrega, and J. Strait
Fermi National Accelerator Laboratory

C. Bromberg, J. Huston, J.P. Mansour, R. Miller, R. Richards, and C. Yosef
Michigan State University

V. Barnes, M. Fahling, A. Laasanen, J. Ross, and Q. Shen
Purdue University

UNIVERSITY OF ROCHESTER

DEPARTMENT OF PHYSICS AND ASTRONOMY

ROCHESTER, NEW YORK 14627

UR-1371/ER40685-821
CDF/DOC/PLUG_UPGR/PUBLIC/2778
Version 2.2
30 September 1994

Quality Control Studies of Scintillating Tile/Fiber Megatile Production for the CDF End Plug Upgrade Hadron Calorimeter

P.de Barbaro, K. Michaud, A. Bodek, H. S. Budd,
Q. Fan, M. Olsson, M. Pillai and W. K. Sakumoto
University of Rochester

M. Albrow, R. Bossert, S. Delchamps, K. Ewald, J. Freeman, J. Kerby,
W. Koska, P.J. Limon, F. Nobrega, and J. Strait
Fermi National Accelerator Laboratory

C. Bromberg, J. Huston, J.P. Mansour, R. Miller, R. Richards, and C. Yosef
Michigan State University

V. Barnes, M. Fahling, A. Laasanen, J. Ross, and Q. Shen
Purdue University

ABSTRACT

We summarize the quality control results of scintillating tile/fiber multi-tile assemblies (megatiles) produced for the CDF End Plug Upgrade Hadron Calorimeter. Approximately 60% of the total number of the 594 30^0 Hadron megatiles needed for the project have been assembled and tested at the FNAL Lab 5 facility. This sample of megatiles corresponds to approximately 12,500 individual tile/fiber assemblies. We discuss the quality control requirements and present the distributions of the quantities measured during the QC process. The various contributions to the tile-to-tile light yield variations are isolated and discussed. The production of Hadron megatiles for the upgraded CDF End Plug Calorimeter is expected to be completed in November 1994.

1. Introduction

A detailed description of the design and construction of the upgraded CDF End Plug Hadron Calorimeter can be found in Ref. [1]. Technical details on construction of the Hadron multi-tile assemblies (megatiles) are described in Ref. [2]. Some of the earlier studies leading to the final design of the optical system for the Hadron calorimeter can be found in Ref. [3]. The results of the 1991 test beam studies of the End Plug prototype calorimeter are described in Ref. [4]. A scintillating tile/fiber system for the upgraded CDF Plug Electromagnetic Calorimeter, which will be located in front of the upgraded End Plug Hadron Calorimeter, is described in Ref. [5].

The production of Hadron megatiles took place in two labs at FNAL. Cutting of scintillator plates and machining of fiber grooves was done using the Thermwood computer controlled mill in Lab 8. Separation grooves between individual tiles were filled with a white paint/epoxy mixture to provide the optical isolation and mechanical strength of the megatiles. After the cutting and glueing operation, the megatiles were wrapped using white reflective paper (*Tyvek*) and light tightening material (*Tedlar*) and sandwiched between precut aluminum sheets. Such pre-assembled megatiles were then shipped to Lab 5. There, the fiber/connector assemblies were prepared and tested. Finally, the fibers were inserted into megatiles and the entire assembly underwent the quality control (QC) test. After passing the QC tests, the megatiles were taped and stored for future assembly of the detector.

The cutting of scintillator plates and pre-assembly of megatiles took place in Lab 8 between June 1993 and June 1994. A full assembly of the Hadron scintillating tile/fiber multi-tile assemblies (megatiles) for the CDF End Plug started at the beginning of December 1993. As of beginning of September 1994, Hadron megatiles for the layers L00 through L13 (14 out of the total of 22 required for the project) have been produced and tested. Figure 1 shows the rate of the assembly of megatiles as a function of time. The rate of megatile assembly was driven by the rate of production of the fiber/connector assemblies and has reached a level of $\approx$ 80 megatiles per month. The entire production and testing of Hadron megatiles is expected to be completed in November 1994. The megatiles will be inserted into the existing steel structure of the CDF End Plug Hadron detector prior to the Run II of the Tevatron Collider.

For each sampling layer of the calorimeter we have to produce 27 30^0 Hadron megatiles. Of these, 24 will be used in the two end plugs. The additional megatiles will be used for the 60^0 test beam module, and as a possible replacement backup. Megatiles from layers L03-L21 are transversely segmented into 32 tiles, and those from layers L00-L02 are segmented into 36 tiles. The transverse segmentation of layer L02 and L03 megatiles is shown in Fig. 2. The readout fibers for each 30^0 megatile are terminated at its radial edge using four connectors, carrying 8 (9 for layers L00-L02) fibers each. Figure 3 shows the numbering scheme of individual tiles used in the quality control analysis presented here.

The QC test of megatiles performed in Lab 5 was a two-step process. After the fibers were mirrored, spliced, and glued into the fiber/connector assemblies, they were tested using a UV setup.[6] Following this test, the fibers were inserted into the tiles, and the assembled megatiles were scanned using two types of radioactive sources. A collimated Cs^{137} γ source was used to establish the quality of the individual tiles. We

also measured the response of the tiles using an uncollimated Cs^{137} γ source[7] (wire source). This measurement allowed us to establish the calibration of the response of tiles to wire source, which will be used in the future tests of the megatiles in the B0 Hall after their assembly into the steel structure of the detector.

In this note we describe the data for layers L00 through L13. A total of 378 megatiles corresponding to 12,420 tiles have been tested and are included in this data set *.

2. Quality Control Measurements

2.1. Quality Control of Scintillator Plates

Prior to the shipment of scintillator material to FNAL, the thickness of each scintillator plate was measured by the manufacturer, Kuraray Int. Corporation.[10] The distribution of the average thickness of scintillator plates is shown in Fig. 4. The nominal thickness of the scintillator SCSN-38 used for the production of Hadron megatiles was 6 mm. Scintillator plates with the average thickness below 5.8 mm were rejected by the manufacturer. The distribution of average scintillator plate thickness had RMS of 1.2%.

In order to measure the variation in the absolute light yield of the scintillator material, we have studied the absorption spectra of Bi^{207} source in scintillator samples. Small, 2 cm $\times$ 2 cm scintillator pieces were put directly onto a face of the PMT (green extended Hamamatsu R580-17, at approximately 950 Volts) and were excited with the β source. Figure 5 shows an example of an ADC distribution of the PMT signal corresponding to the absorption spectrum of Bi^{207}. The light yield of each scintillator sample, relative to the reference sample, was measured by determining the position of the highest absorbtion peak in the spectrum. Figure 6 shows the distribution of the light yield of a set of scintillator samples, relative to the reference sample, as determined from the Bi^{207} spectrum. From this plot we infer that the distribution of the absolute light yield of scintillator plates had RMS of 1.6%.

2.2. UV Fiber Test

The optical readout fibers were tested after they were mirrored, spliced, and assembled into mass-terminated connectors. Figure 7 shows the rate of production of fiber/connector assemblies as a function of time. A total of approximately 2600 fiber/connector assemblies is needed for the completion of the CDF End Plug Hadron Calorimeter project.

The fibers were tested by exciting them with an UV lamp and measuring their response using a photodiode/picoampmeter/PC setup. The lamp was moved in small steps along the length of the fibers and the response of the diode was recorded. The peak wavelength of the UV lamp used in this setup was 405 nanometers (nm). A blue filter was used to remove the harshest UV light of wavelength less than 385 nm. By measuring the light yield of individual fibers, we checked the quality of the polishing, reflectivity of

*This data set does not include the response of two of the lowest η tiles (tiles 33 and 35). This data will be included following installation of the Had+EM descrambler, used to route light from individual tiles to the four readout PMTs.

the mirror surface, the light transmission across the splice between wavelength shifter (WLS) and clear fibers, and the quality of the connector surface.

Figure 8 shows the distribution of the relative light yield of fibers as measured by the UV setup. The RMS of this distribution is 3.2%. Fiber light yield was normalized to the average light yield of the set of fibers with the same length. For example, for layer L13 we used 32 calibration constants, each equal to the average light yield of 27 same-length fibers. The fibers with the relative light yield less than 12% below the average were rejected. In those few cases, the particular green fiber was replaced and the entire connector was tested again. In some cases the low light yield of a fiber was related to a problem associated with clear fibers or connector parts. In these particular cases, the entire fiber/connector assembly was discarded and replaced by a new one. During the discussed production period, we have produced approximately 1600 fiber/connector assemblies containing over 12,500 fibers. In this sample, 85 fibers ($\approx 0.7\%$) were respliced and 40 connectors ($\approx 2.5\%$) were rejected.

The above described QC tests do not directly measure the light transmission across the WLS-to-clear fiber splice nor the mirror reflectivity. In order to directly monitor these parameters special tests were periodically performed. The light transmission across fiber splices was measured once per week or after any work performed on the splicing machines. The mirror reflectivity was measured for each batch of mirrored fibers.

The light transmission across a splice can be best measured by studying the splices between two green WLS fibers. We first scanned a set of long green WLS fibers with no splices present. We then cut each fiber, polished the ends and spliced the fibers, keeping the cut fiber pairs matched. We then measured the ratio of light yields for these two scans and determined an average light yield transmission across the splice. Figure 9 shows the light transmission across green-to-green fiber splices for the sample of fibers tested during the discussed production period. The average light transmission across the splice of two WLS fibers is 92%, with the RMS of the distribution of $\approx 3\%$. It should be pointed out that during the discussed production period, we have used two splicing machines. Thus the variation in the light transmission across fiber splices in Fig. 9 includes the effects of combining distributions with different means from each splicer. The systematic difference in the quality of different splicing machines was estimated to be between 1% to 2%.

The fibers were aluminized in a bell jar system utilizing either a 3 inch or a 4 inch magnetron sputtering gun driven by a DC power supply. For good reflectivity, we used 99.999% chemically pure (five nines) aluminum targets. The sputtering process was started after achieving a low 10^{-6} Torr vacuum, and then backfilling with "sputtering grade" Argon gas back up to 5 milliTorr (5 microns) pressure. The coating was approximately 2500 Angstroms thick and was monitored using an oscillating quartz crystal sensor device. The fiber ends were placed 6.5 inches away from the surface of the aluminum target with mylar and kapton packaging used to protect the rest of the fibers from being coated.

The mirror reflectivity was measured by a destructive test using fibers which were mirrored at the same time as the fibers used for the Hadron megatile production. The fibers were first measured using the UV setup with the mirrored ends intact. The

mirrored end of each fiber was then cut off, approximately 1 mm from the end, at a 45° angle and painted black. The light yield of fibers was measured again. In both of these measurements, the UV lamp was positioned near the mirrored end of the fibers. The ratio of these two light yield measurements was then used to determine the reflectivity of the mirror. Figure 10 shows the distribution of the reflectivity of the fiber mirrors tested during the discussed production period. The low readings ($< 80\%$, marked with cross-hatched area on the figure) occurred during a period when the sputtering was known to be bad. Fiber batches mirrored during this particular period were not used for the production of the connector assemblies for the CDF End Plug.

The average mirror reflectivity, excluding the fibers mirrored during the period of the sputtering machine problems, was equal to 90%, with RMS of this distribution of 5.4%. However, due to the attenuation of light in green WLS fibers, the typical increase of light yield of fibers with mirrored ends was between 30 to 40%. Thus, the contribution to the variation of the fiber light yield originating from the variation in the mirror reflectivity was $\approx 1.5\%$.

2.3. Collimated Cs^{137} γ Source Test

After passing the UV light yield QC test, the fibers/connector assemblies were inserted into the megatiles. Next, the megatiles underwent the QC tests using the collimated Cs^{137} γ source. We used a PC controlled motor system and data aquisition system to record the response of individual tiles to the radioactive source. The megatiles were placed inside the light-tight scanner box and positioned against three alignment pins. The relative light yield of the tiles was measured by using a set of photomultiplier tubes † (PMT) for the readout and recording their DC current response. The data was taken in sequence by moving the source over the geometrical center of each of the tiles in a megatile.

In order to minimize the number of PMTs used, the entire megatile was read out using only four PMTs arranged in a double-checkerboard pattern, as shown in Fig. 3. In this particular arrangement, tiles adjacent to each other were read out by different PMTs. Such an arrangement allowed us to reduce the number of PMTs used in the test, at the same time keeping contributions to PMT signals from adjacent tiles at few percent level.

The dark current, or pedestals of each PMT were monitored by recording the response of the PMTs with the radioactive γ source located away from the tiles. To monitor the stability of the PMT gains, we used eight control tiles (two per PMT). The control tiles were permanently connected to the PMTs and were not subject to connect/disconnect procedure between subsequent megatile measurements. The quality control test of each megatile consisted of the following measurements: the PMT pedestal and gain stability measurement, the sequence of individual tile measurements, followed by another PMT pedestal and gain measurement. In addition we also recorded the temperature inside the scanner box using four temperature sensors.

Figure 11 shows the distribution of the pedestal values of each of the four PMTs used in the measurement. The PMTs had typical pedestals of $\approx 1\ nA$ with a variation

†Hamamatsu R580-17, 10-stage, green-extended PMTs, operated at HV of approximately 1350 V, corresponding to a 10^6 gain.

(RMS) of $\approx 0.1nA$. Since a typical signal from a tile was $\approx 50 - 70\ nA$, the pedestal variations contributed to the measurement error at a level below 0.2%.

As mentioned above, the gains for the PMTs were monitored before and after each megatile test using the control tile setup. Figure 12 shows the distribution of the relative gain of the four PMTs. The RMS of the relative gain of each tube measured during the period of QC tests described here (Dec. '93 through Aug. '94) was $\approx$ 0.7% to 1.0%. Figure 13 shows the relative gain of each PMT plotted as a function of temperature inside the scanner box. The change of the PMT gain was strongly correlated with the temperature change. In order to determine the temperature coefficient of the PMT gain variation, we have fitted the above data to a first degree polynomial (see Fig. 14). The relative variation in PMT gain was -0.3%, -0.6%, -0.4% and -0.6% per ^{o}C for the 4 PMTs used. After correcting each PMT gain for the temperature dependence, the residual gain variation of the PMTs was between 0.5% and 0.7%, as shown in Fig. 15.

To define the signal of each tile, we first correct the pedestal-subtracted signals (DC readings) for the PMT gain variation as measured by the response of the control tiles. We then define the relative light yield of a tile as its signal normalized to the average signal of all tiles from the same layer and tower. For example for layer L13, comprising of total of 864 individual tiles, we have used 32 calibration constants, each equal to the average of 27 measurements of tiles from the same tower.

Figure 16 shows the distribution of the relative tile light yield for individual tiles from layers L00 through L13. The RMS of this distribution is 6.1%. Few tiles with relative light yield less than 78% below the mean were repaired. In such cases, we have either respliced its WLS fiber or replaced the entire fiber/connector assembly. During the discussed production period (total of 378 megatiles produced, with 1512 connectors and 12,420 fibers), 36 fibers ($\approx$ 0.3%) had to be respliced and 26 ($\approx$ 1.7%) connectors had to be replaced. Therefore, after the two QC tests (the UV fiber light yield test and the collimated γ source megatile light yield test), a total of 1% of fibers were respliced and a total of 4% of fiber/connector assemblies were rejected and replaced.

2.4. Sources of Relative Light Yield Variation

We can define the total variation of the relative tile light yield distribution, σ_{tot}, as:

$$\sigma_{tot}^2 = \sigma_{fib}^2 + \sigma_{meg}^2 + \sigma_{other}^2 \qquad (1)$$

where σ_{fib} is the relative fiber light yield variation and σ_{meg} is the average megatile light yield variation. We define the average megatile light yield as an average relative light yield of all 32 tiles belonging to the same megatile. The σ_{meg} describes the additional contribution to the tile light yield variation due to systematic factors common to all tiles cut from the same scintillator plate. The σ_{other} corresponds to the light yield variation due to other factors. These factors include the quality of optical coupling of fibers inside the megatile and local variations in the scintillator material thickness.

As shown in Fig. 16, the total width of the relative light yield distribution of tiles, σ_{tot}, is equal to 6.1%. We show below that the contributions to σ_{tot} originating from the fiber light yield variation (σ_{fib}) were equal 3.2%, contributions originating from the systematic megatile light yield variation (σ_{meg}) were equal 3.6%, and contributions due to other factors (σ_{other}), were equal to 3.7%.

Figure 17 shows the average relative tile light yield, as a function of the relative fiber light yield. In the above plot, the relative tile light yield was measured using the collimated γ source and the relative fiber light yield was measured by the UV setup. The strong correlation indicates that the tiles containing high light yield fibers will on average give a higher light yield than tiles read out with lower light yield fibers. We can determine the effect of the fiber light yield variation on the total tile light yield variation. Figure 18 shows the distribution of the relative tile light yield divided by the relative fiber light yield. The RMS of this distribution is 5.3%. This is consistent with 5.2% variation obtained by subtracting in quadrature the σ_{fib} equal to 3.2% from σ_{tot} equal to 6.1%.

We can determine the systematic correlation in the light yield of tiles built from the same scintillator plate by studying the average megatile light yield. If there were no such correlations, the width of distribution of the average of 32 tiles in each megatile should be equal to $\approx$ 1.1% (from statistical arguments, we can calculate it by dividing the tile light yield RMS of 6.1% by $\sqrt{32}$). The distribution of the average megatile light yield for 378 measured megatiles is shown in Fig. 19a. The RMS of this distribution is 3.6%, significantly larger than 1.1%, indicating a systematic correlation in the light yield of tiles from same megatiles [‡]. The possible factors contributing to the variation of the average megatile light yield include the systematic variation in the thickness of scintillator plate and its absolute light yield, as well as the systematic variation in the quality of the grooves holding the WLS readout fibers.

As discussed in Sec. 2.1, since the light yield of scintillator samples was determined using the position of the β source absorption peak, its variation was not sensitive to the variation in the thickness of scintillator samples. Therefore, the combined variation in the thickness of the scintillator plates (RMS equal to 1.2%, as shown on Fig. 4) and the variation in the absolute light yield of scintillator (RMS equal to 1.6%, as shown on Fig. 6) contributes 2% to σ_{meg}, the systematic variation in the light yield of tiles from same megatiles, equal to 3.6%.

Therefore we conclude, that there must be additional sources of the variation of average megatile light yield beyond variations in the average thickness and absolute light yield of scintillator plates. Certain processes, such as milling of fiber grooves, painting of tile edges with white paint or filling the separation grooves with white paint/epoxy mixture were performed at the same time for all the tiles from same scintillator sheet.

During the megatile production process in Lab 8, two 30^0 megatiles were cut from each rectangular scintillator sheet. Therefore systematic variations in the quality of fiber grooves or variations in the reflectivity of white paint and white paint/epoxy mixture would lead to the correlation in the average megatile light yields of two megatiles cut from the same scintillator sheet.

Figure 20 shows the scatter plot of the average light yields of pairs of megatiles cut from same scintillator plates. The correlation between the average light yields of two megatiles cut from same scintillator sheet indicates that indeed one of the produc-

[‡]We should note, that the distribution of the average fiber light yield (per each assembled megatile) has RMS of $\approx$ 1%, only slightly above 0.6% expected for the fully uncorrelated distribution ($3.2\%/\sqrt{32}$), see Fig. 19b.

tion processes taking place in Lab 8 (cutting of fiber grooves, painting the tiles edges with white paint and filling the separation grooves with white paint/epoxy mixture) contributed to the variation in the average megatile light yield. Number of tests are presently underway to further understand the source of this variation.

Figure 21 shows the distribution of the relative tile light yield divided by both the relative fiber light yield and the average megatile light yield. The width of such a distribution is sensitive to the variations in the optical coupling of individual fibers to scintillator material, as well as the measurement errors of fiber and tile light yields. The RMS of the distribution is 4.3%. The RMS width of this distribution is indeed consistent with the σ_{other}, as defined using the equation (1):

$$\sigma^2_{other} = \sigma^2_{tot} - \sigma^2_{fib} - \sigma^2_{meg} \qquad (2)$$

Using values of σ_{tot}, σ_{fib} and σ_{meg} as derived from Fig. 16, 8 and 19 respectively, the value of σ^2_{other} is equal to: $(6.1\%)^2$ - $(3.2\%)^2$ - $(3.6\%)^2$, yielding σ_{other} equal to 3.7%.

3. Front-to-Back Relative Light Yield Variation

In addition to studying the overall width (RMS) of the distribution of relative light yield of tiles, it is important to determine the average light yield of tiles as a function of the layer number. A systematic variation in light yield of tiles from the inner (front) layers relative to the outer (back) layers (sometimes referred to as front-to-back slope) could contribute to the degradation of the energy resolution of the calorimeter.[8]

As described in the detail in Ref. [1], in order to minimize the front-to-back slope in the average response of tiles, we have adjusted the distance between the edges of tiles and the σ fiber groove inside the tile. In addition, the average light yield of tiles was adjusted by a suitable choice of the position of WLS-to-clear fiber splice.

Figure 22 shows the average light yield of tiles, plotted as a function of layer number. Layer 0 is the inner-most (front) layer, following the EM calorimeter, and layer 21 is the outer-most (back) layer of the Hadron calorimeter. The data was normalized relative to the average light yield of a subset of L21 and L20 megatiles. The error bars on the plot are statistical only. A systematic underestimate of up to 5% for the front-most layers may be present, due to the finite size of the lead cone used to collimate the Cs^{137} γ source. The plot indicates a general decrease in the average tile light yield as the layer number increases, stabilizing for the layers L13 and higher.

It is important to realize, that the tiles from various layers were tested using a same length optical cable (4 meters long), placed between the outer edge of the megatiles and the readout PMTs. However, in the future, following the installation of megatiles into the steel structure of the detector, the inner layers will be read out using longer clear optical cables than the outer layers. The dashed line on Fig. 22 shows the effect of the light attenuation of the clear fibers ($\lambda^{cl}_{att} \approx 7.4$ m) on the average light yield of tiles. In addition, the final light yield of tiles after installation in the B0 hall, will be affected by the magnetic field present inside the calorimeter. The strength of magnetic field increases from negligible values for the outer most layers to 1.4 T for the inner most layers. Thus it increases the light yield of inner-most layers[9] by up to 10%, as shown by the dot-dashed line on Fig. 22.

Figure 23 shows the expected average light yield of tiles as a function of layer number, after accounting for the two above described effects, the attenuation length of

the clear optical cable and the effect of the magnetic field inside the hadron detector. As shown on the plot, the expected variation in the average light yield is within $\pm 10\%$ band, and as the preliminary studies indicate,[8] would not significantly contribute to the degradation of the energy resolution of the Hadron calorimeter.

4. Wire source vs collimated source measurements

As mentioned earlier, in addition to testing the megatiles with the collimated γ source, each megatile was scanned using an uncollimated γ source. The source was located at the end of a wire which was inserted during the measurements into steel tubes embedded in each megatile. The layout of steel tubes inside plastic covers placed above the scintillator sheets is depicted on Fig. 2. The steel tubes allowed us to guide the γ source over the geometrical center of individual tiles.

The PMT signal was recorded as a function of position of the wire source inside the megatile. Individual tile responses were then determined using a peak-finding algorithm. The reproducibility of the peak finding procedure was determined by studying the ratio of tile response as measured during the extension and the retraction of the wire source into the megatiles. As shown of Fig. 24, the RMS of this distribution is 0.6%.

Studying the ratio of wire source vs collimated source tile light yields, normalized separately for each layer and tower, $R^{rel}_{w/c}$ was an effective approach to check the consistency of the QC data. Note, that due to the normalization used, the $R^{rel}_{w/c}$ is not sensitive to the effect of the variation in the size of tiles from various layers and towers. The small RMS ($\approx 1.2\%$) of the ratio of the wire source to the collimated source light yield measurement implied that the positioning of the steel tubes used to guide the wire source along the surface of megatiles was well controlled and did not introduce a large uncertainty to the wire source measurements. In a few cases, the $R^{rel}_{w/c}$ was 5% or more away from the average, indicating a possible inconsistency of the QC data for a particular megatile [§].

By comparing the ratio of the wire source tile light yield over the raw collimated source tile light yield, $R^{raw}_{w/c}$, most of the contributions to tile light yield variations cancel as both light yield measurements are subject to the same variations (fiber light yield, scintillator light yield, optical couplings) for each particular tile. The average $R^{raw}_{w/c}$ is therefore only sensitive to the fact that as the size of tiles increases, the amount of the radiation received by the tiles from the wire source increases, while the amount of radiation received from the collimated source is fairly constant. By measuring the $R^{raw}_{w/c}$, we therefore establish a calibration for the future wire source measurements of tiles, to be taken after the installation of megatiles into the steel structure of the hadron detector.

Various tiles in each megatile have different areas. Figure 26 shows the plot of area of tiles from layer L06, as a function of their *Tile ID*, assigned according to Fig. 3.

[§]Possible ways that the megatiles could be tested incorrectly include having the incorrect voltage applied to the PMTs; having the megatile's fiber connectors not properly latched to the readout cables; not having the megatile accurately aligned against the alignment pins during testing; and having the wire source tubes not properly connected. Once rescanned by the collimated source and the wire source, the high rms no longer existed.

Figure 27 shows the ratio $R^{raw}_{w/c}$, as a function of the tile size for layer L06 tiles. The variation in the area of the tiles is the main source in the variation of the ratio $R^{raw}_{w/c}$. Two distinct lines in the $R^{raw}_{w/c}$ vs tile area correspond to sets of tiles with different aspect ratio (ratio of width to height for the 15^0 and 7.5^0 ϕ segmentation of the megatiles).

Figure 28 shows the $R^{raw}_{w/c}$ for two towers with 15^0 ϕ segmentation, towers 12 and 28 (for tower number assignment, see Fig. 3). The plots indicate the increase of this ratio as a function of increasing layer number, and thus increasing tile sizes. We have used a volume integral calculations to predict the dependence of the ratio of the wire source to collimated source tile response[11] as a function of the size of a tile. The calculations were able to reproduce the measured ratios to better than 1%.

5. Optical Cross-talk between Adjacent Tiles

As mentioned earlier, individual tiles constituting a 30^0 megatile were joined together using a white paint/epoxy mixture.[2] Such procedure provided both, the mechanical strength of the assembly, as well as the optical isolation between the neighboring tiles. The cross-sectional view of a region between two neighboring tiles is shown in Fig. 29. During the production, the separation grooves between the tiles were cut using a 0.035 inch (0.9 mm) diameter bit. The 6 mm thick scintillator plate was not cut entirely apart, leaving approximately 0.2 mm of uncut material below the separation groove. The uncut material allowed us to maintain the mechanical integrity of the entire megatile, until the separation grooves were filled with white paint/epoxy mixture.

However, the uncut scintillator material, approximately 3% of the total thickness of the scintillator plate, introduced the optical cross-talk between the neighboring tiles. We define the optical cross-talk between two neighboring tiles as the light yield of a particular tile when the source is placed on a neighboring tile normalized to the light yield with source placed on the center of the tile. Due to the finite size of the lead absorber used to collimate the γ source, a small amount of radiation from the source excited the neighboring tiles directly. This radiation cross-talk was determined to be between 0.7% to 0.9% and was subtracted from the total cross-talk measured between the neighboring tiles.

Figure 30 shows the dependence of the optical cross talk between two tiles as a function of thickness of the uncut material below the separation groove. As the open symbols indicate, the cross-talk strongly depends on the thickness of the uncut material, and in case of 6 mm thick scintillator tiles, is equal $\approx$ 2% for the 0.2 mm of uncut material and $\approx$ 5% for 0.4 mm of uncut material.

In order to suppress the optical cross-talk between neighboring tiles and reduce its sensitivity to the thickness of uncut material, we apply a permanent black marker line below the area of the separation groove. The dark symbols on Fig. 30 indicate the optical cross-talk between neighboring tiles after the application of black marker line, $\approx$ 2 mm wide, below the tile separation groove. By absorbing the light, the black line reduced the optical cross-talk to the level below 1% and made it much less sensitive to the thickness of uncut scintillator material.

Figure 31 shows the distribution of the thickness of uncut material for a sample of scintillator plates used in the production of layer L18 of Hadron megatiles. The thickness of uncut scintillator in the separation groove varied between 0.15 to 0.3 mm,

with the average equal to 0.2 mm. Figure 32 shows the distribution of the optical cross-talk between neighboring tiles, as measured during the QC tests of Hadron megatiles. The optical cross-talk varied between 0 to 2%, with the average equal to $\approx$ 1%. Such values of optical cross-talk will not degrade the performance of the Hadron calorimeter.

6. QC Data Base for Hadron Megatiles

The data collected during the QC tests of megatiles produced for the CDF End Plug Upgrade Hadron Calorimeter is stored as a *FoxPro* data base file.[12] The data base contains the information on the quality of the scintillator plates from which individual tiles were cut, such as material thickness and its absolute light yield, information on the quality of the fiber material used to produce fiber/connector assemblies as well as the individual QC measurements of fibers after the construction of the fiber/connector assemblies and QC tests of the assembled megatiles. A separate memo[13] describes the technical details of the data base setup.

7. Summary

We have measured the overall variation in the light yield of tiles used for the CDF Plug Upgrade Hadron calorimeter. The total width of this distribution (σ_{tot}) is 6.1%, with approximately 3.2% coming from the variation in the performance of readout fibers (σ_{fib}), 3.6% from the systematic variation in light yield of tiles (σ_{meg}), and 3.7% due to other effects, such as tile/fiber optical coupling. The RMS of 6.1% is within the design goal of the end plug upgrade hadron calorimeter.

We have also studied the systematic variation in the average light yield of tiles from different layers of the Hadron calorimeter. The ratio is $\pm$ 10% within unity and meets the linearity design criteria of the calorimeter.

The optical cross-talk between neighboring tiles is below 2% and will not contribute to the degradation of the performance of the Hadron calorimeter. The QC studies also indicate that the wire sources can be used to calibrate the response of individual tiles with accuracy of $\approx$ 1.5%.

Acknowledgements

We thank all of the Fermi Lab staff and technicians who worked on the Hadron calorimeter megatile construction and testing in Lab 8 and Lab 5. They have all done superb and excellent job.

First we thank Chuck Serritella and Charlie Hess for their hospitality in Lab 8 and Lab 5 buildings. We thank Rick Dixon and Bob Andree for their work on designing and creating the CAD/CAM files for the Hadron megatiles. We acknowledge the effort of people involved in operations of the Thermwood milling machine and cutting of the scintillator sheets: Scott Carlson, Phyllis Deering, Luis Morris and Jerry Taccki. We would like to thank Anita McKinsey, Edna Turner and Lupie Rodriquez for their work in glueing and packaging the megatiles in Lab 8.

Thanks to Eileen Hahn and Rene Jones for their effort in getting all the WLS fibers mirrored. We thank Jill Calderon, Scott Doerr. Pete Gutierrez, Charlie Paul, Modeste Phelps, Ines Ramos, Pam Schmidt, Dale Sherwin and Ewa Skup for the preparation of fiber/connector assemblies. We appreciate the work of Imre Gonczy and Mike Nurczyk in preparing the parts needed for final megatile assembly. We thank Ethel Gonczy for the work she has done on the fiber insertion and assembly of megatiles. Thanks to Jim Rogers and Sergio Sanchez for their work on final taping of megatiles.

We thank Ken Gray and Jim Tweed for their assistance in building various counters and PMT mounts required for the megatile QC setup. Lastly, we thank Lee Simmons for the design work of the megatile scanner and descrambler boxes and Marty Whitson for the excellent job of performing the QC tests of assembled megatiles.

References

1. The detailed description of the CDF End Plug Hadron Calorimeter can be found in: P. de Barbaro et al., *CDF Plug Upgrade Hadron Calorimeter Design*, U. of Rochester preprint UR-1360, CDF Note 2545 (May 1994).
2. Technical details on construction of the Hadron calorimeter are described in: M. Olsson et al., *Techniques for Optical Isolation and Construction of Multi-Tile Assemblies in Scintillator Tile-Fiber Calorimeters Using White Epoxy*, CDF Note 2582, UR-1370 (Aug. 1994).
3. Earlier publications on R&D results on tile/fiber calorimetry include:
   P. de Barbaro et al., *R&D Results on Scintillating Tile/Fiber Calorimetry for the CDF and SDC detectors*, UR-1229 (Sep 1992), NIM **A315** (1992) 317.
   P. de Barbaro et al., *Recent Results on Tile/Fiber Calorimetry*, UR-1299 (Jan 1993), SDC-93-407.
   G. Apollinari, P. de Barbaro, M. Mishina, *CDF End Plug Calorimeter Upgrade Project*, UR-1329 (Sep 1993), FERMILAB-CONF-94-030-E.
   P. de Barbaro et al., *Study of Light Yield and uniformity in Hadron Calorimetry utilizing Tile/fiber Technology*, UR-1354 (Apr 1994).
4. The results of 1991 test beam of the prototype calorimeter of the CDF End Plug can be found in:
   M.A. Lindgren, *The CDF Plug Calorimeter Upgrade*, in Proceedings of the Third International Conference on Calorimetry in High Energy Physics, Corpus Christi, TX, 29Sep-2Oct92, eds. P.Hale and J.Siegrist, (World Scientific, Singapore 1993).
   J. Hauser et al., Nucl. Instr. & Meth. **A321** (1992) 497, *A Scintillating Fiber Detector for Electron and Photon Identification at High Luminosity Colliders.*
   J. Freeman et al., *The CDF Upgrade Calorimeter*, in Proceedings of the Second International Conference on Calorimetry in High Energy Physics, ed. A.Ereditato (World Scientific, Singapore 1992), p. 189.
5. S.Aota et al., *A Scintillating Tile/Fiber System for the CDF Plug Upgrade EM Calorimeter*, CDF Note 2431 (Mar 1994), to be published in **NIM**.
6. J. P. Mansour et al., *A Semi-automated Splicer for Plastic Optical Fibers*, to be published in Proceedings of the 1993 Scintillating Fiber Workshop, Notre Dame, IN, Nov 5-12 1993.
7. Description of the calibration technique using the wire source setup can be found in: *Proposal for an Upgraded CDF Detector*, Oct 1990, CDF Note 1172.
8. P. de Barbaro, A. Bodek and B. Winer, *The Effects of Tile Miscalibrations on the Performance of Tile/fiber based Hadron Calorimeter*, U. of Rochester preprint UR-1301 (Jan 1993).
9. J.Mainusch et al., Nucl. Instr. and Methods, **A312** (1992) 451;
   D.Blömker et al., Nucl. Instr. and Methods, **A311** (1992) 505.
10. Kuraray International Corp., 200 Park Ave., New York, NY 10166.
11. M. Fahling, Purdue University, private communication.
12. *FoxPro*, Version 2.5. *FoxPro* is a trademark of the Relational Database Management System for Apple Macintosh by Microsoft Co., One Microsoft Way, Redmont, WA 98052-6399.
13. P. de Barbaro and K. Michaud, CDF Note 2783, in preparation.

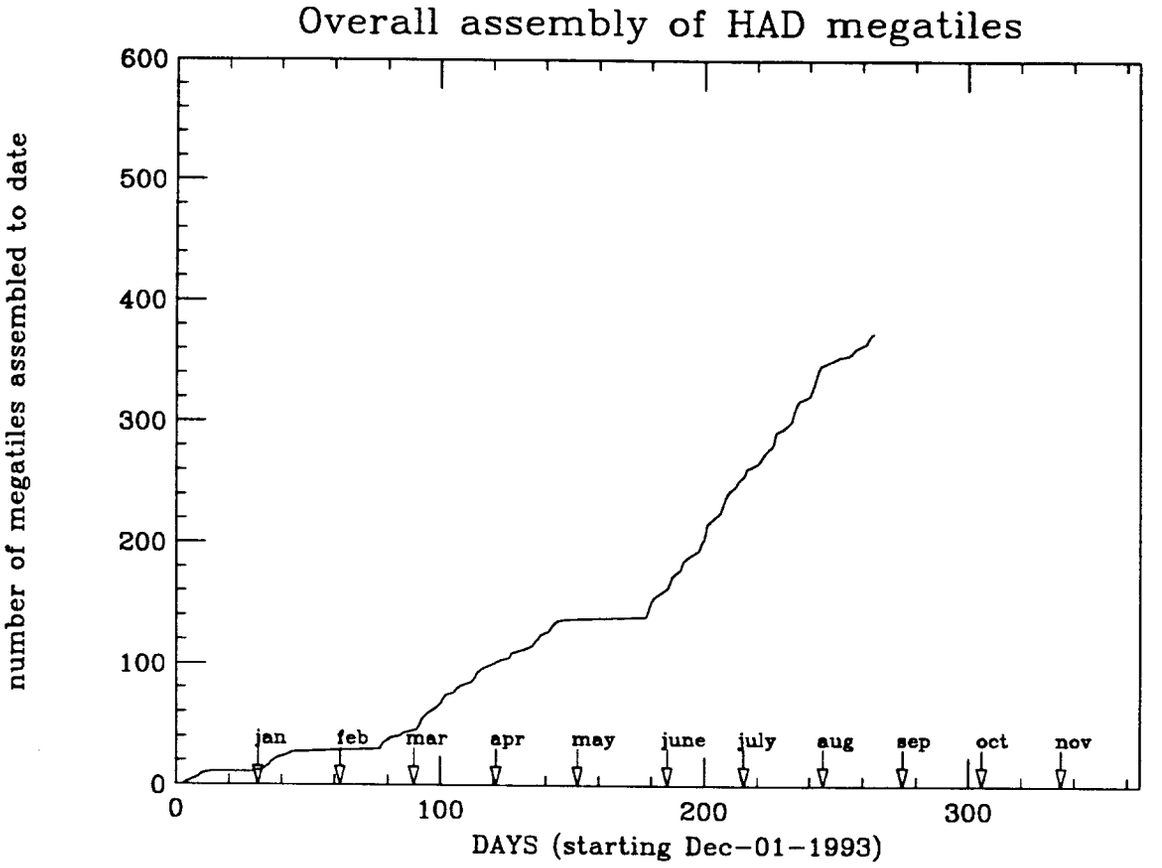

Fig. 1. Megatile production in Lab 5 from December 1993 through August 1994. Assuming a constant work force for the remaining part of the construction, the projected date of megatile completion is November, 1994. There are currently eight full time technicians working on the production and testing of fiber/connector assemblies and four technicians working on the final assembly and megatile testing.

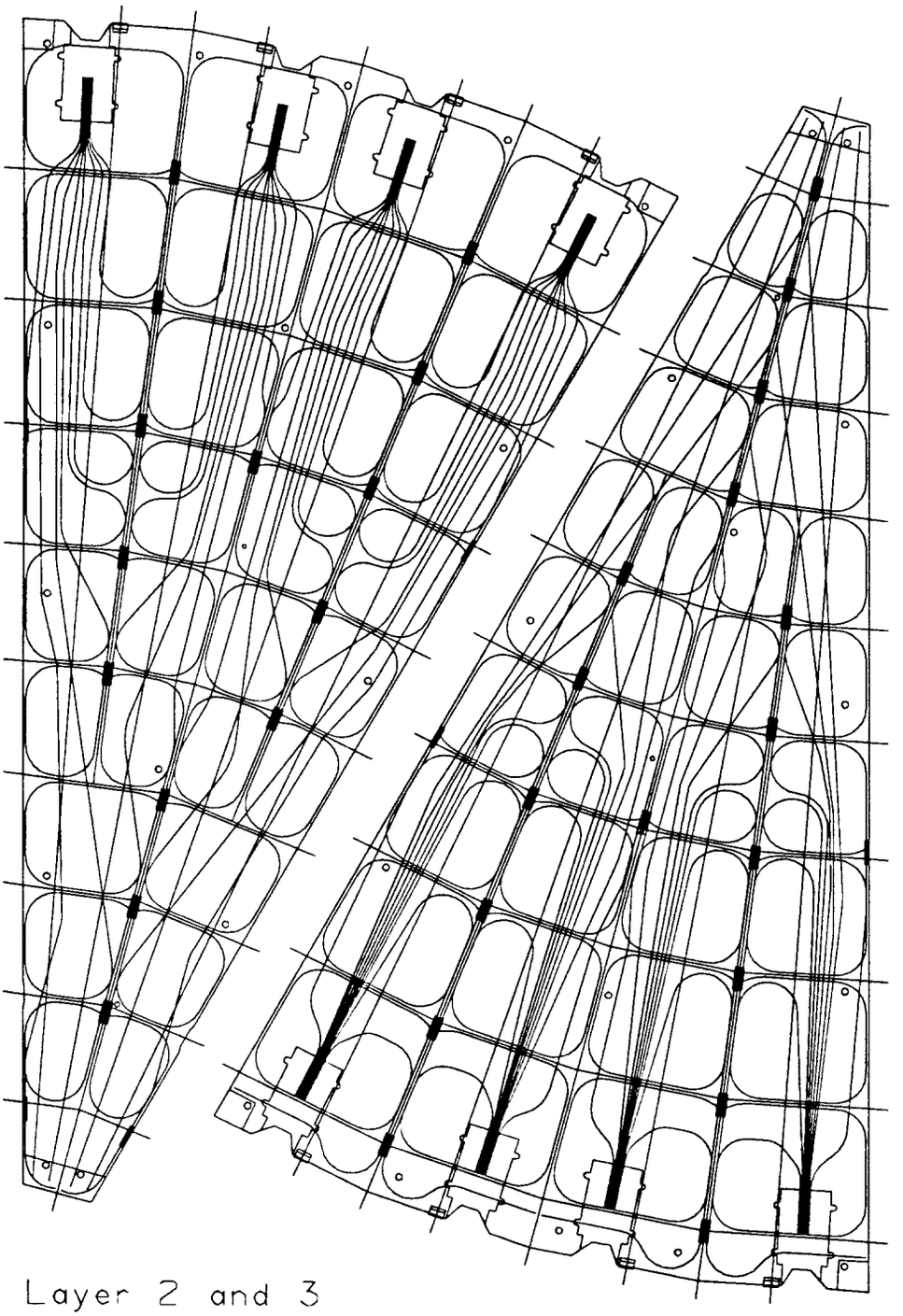

Fig. 2. A diagram of two megatiles, one from layer L02 and one from layer L03. Layer L03 megatile is segmented into 32 tiles in 10 pseudorapidity (η) regions and has eight fibers for each of the four connectors. Layer L02 megatile is segmented into 36 tiles in 11 pseudorapidity regions and has 18 distinct fibers for each 15° symmetric side. During the QC test, the four fiber connectors are attached to four 4 m clear optical fiber cables (not shown on the drawing) to carry light to the PMTs. The four wire source tubes bisect 7.5^0 sections of the megatile and run down the center of each tile.

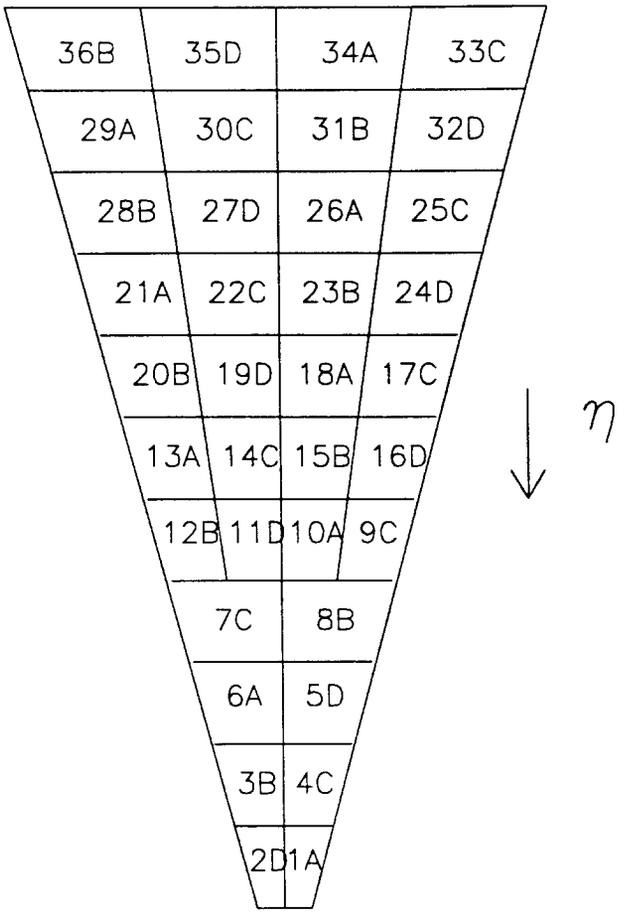

Fig. 3. Diagram of megatile tile numbering system and the 'double-checkerboard' routing scheme of light to the readout PMTs. The arrow at the right hand side of the drawing indicates the direction of increasing η. Tiles 33 through 36 exist only for layers L00 through L02. The numbers correspond to the tile ID convention used in QC tests, and the letters (A, B, C and D) correspond to the PMT assignment used in the readout of a particular tile.

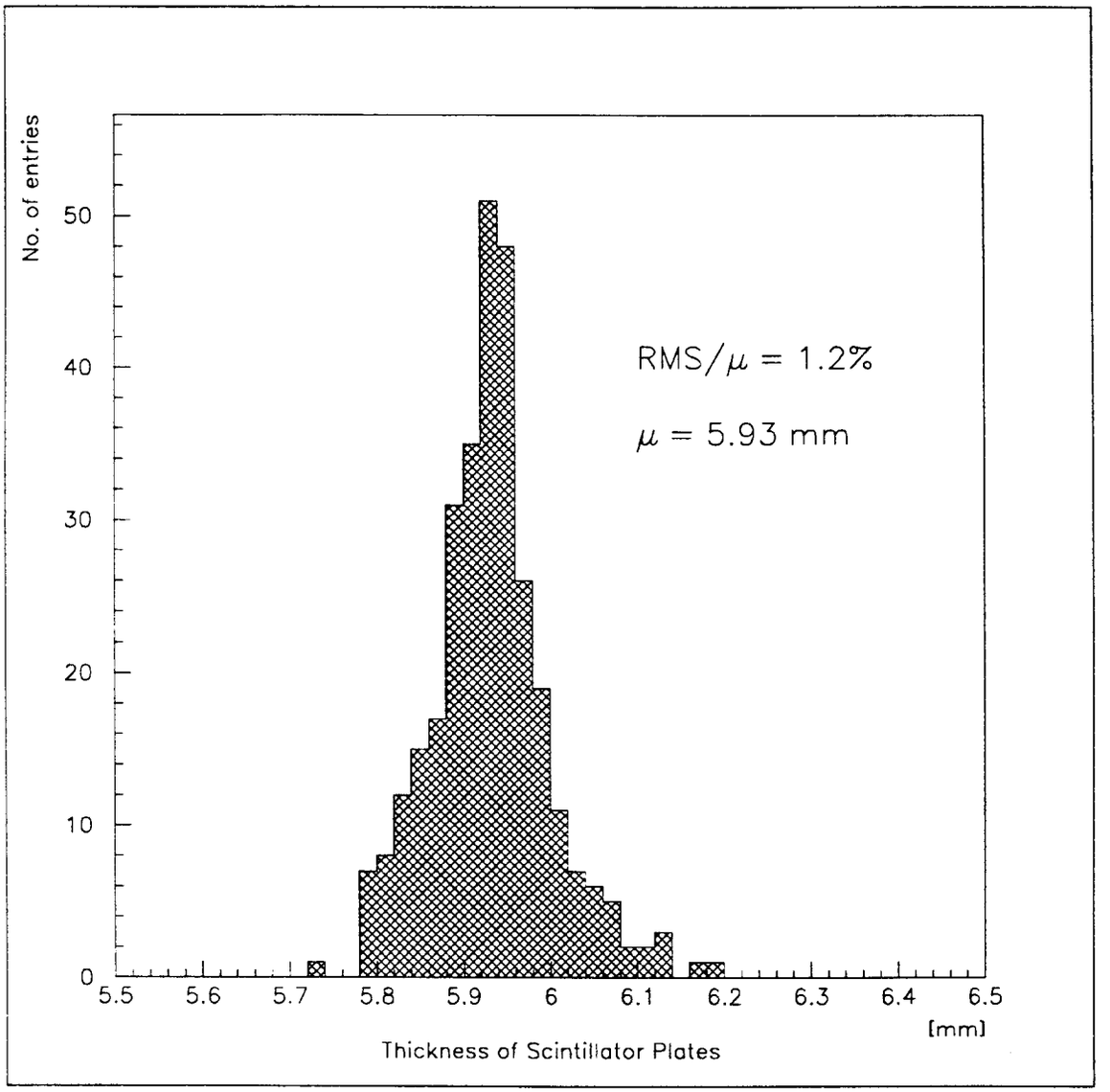

Fig. 4. The distribution of the average thickness of scintillator plates used in the production of Hadron megatiles. The average thickness of plates was 5.93 mm, with RMS of the distribution of 1.2%. The sharp cutoff below 5.8 mm corresponds to the QC cut applied by the manufacturer.

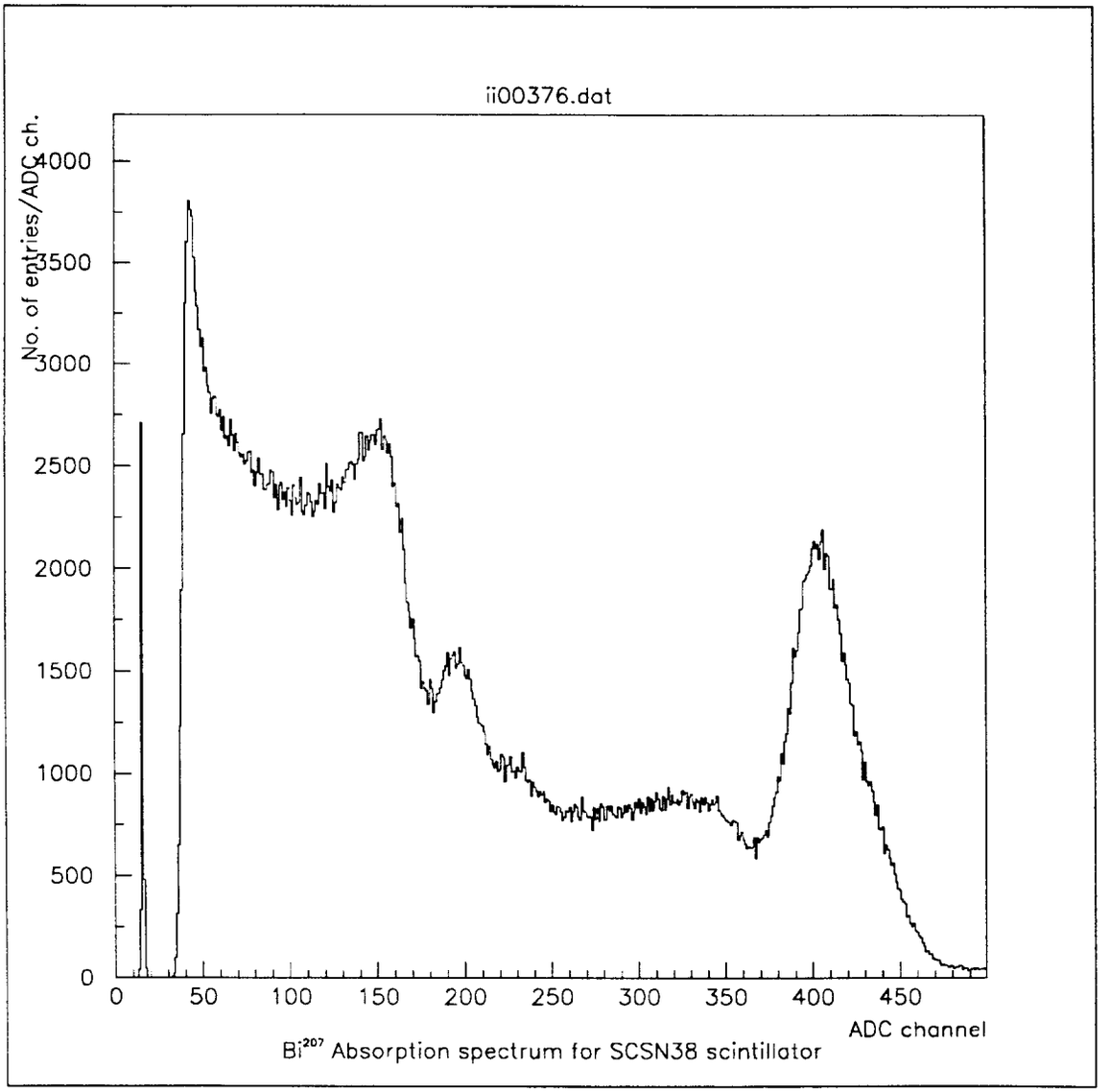

Fig. 5. The absorption spectrum of the Bi^{207} β source in the SCSN-38 scintillator. The position of the highest peak was used to determine the relative light yield of the scintillator samples.

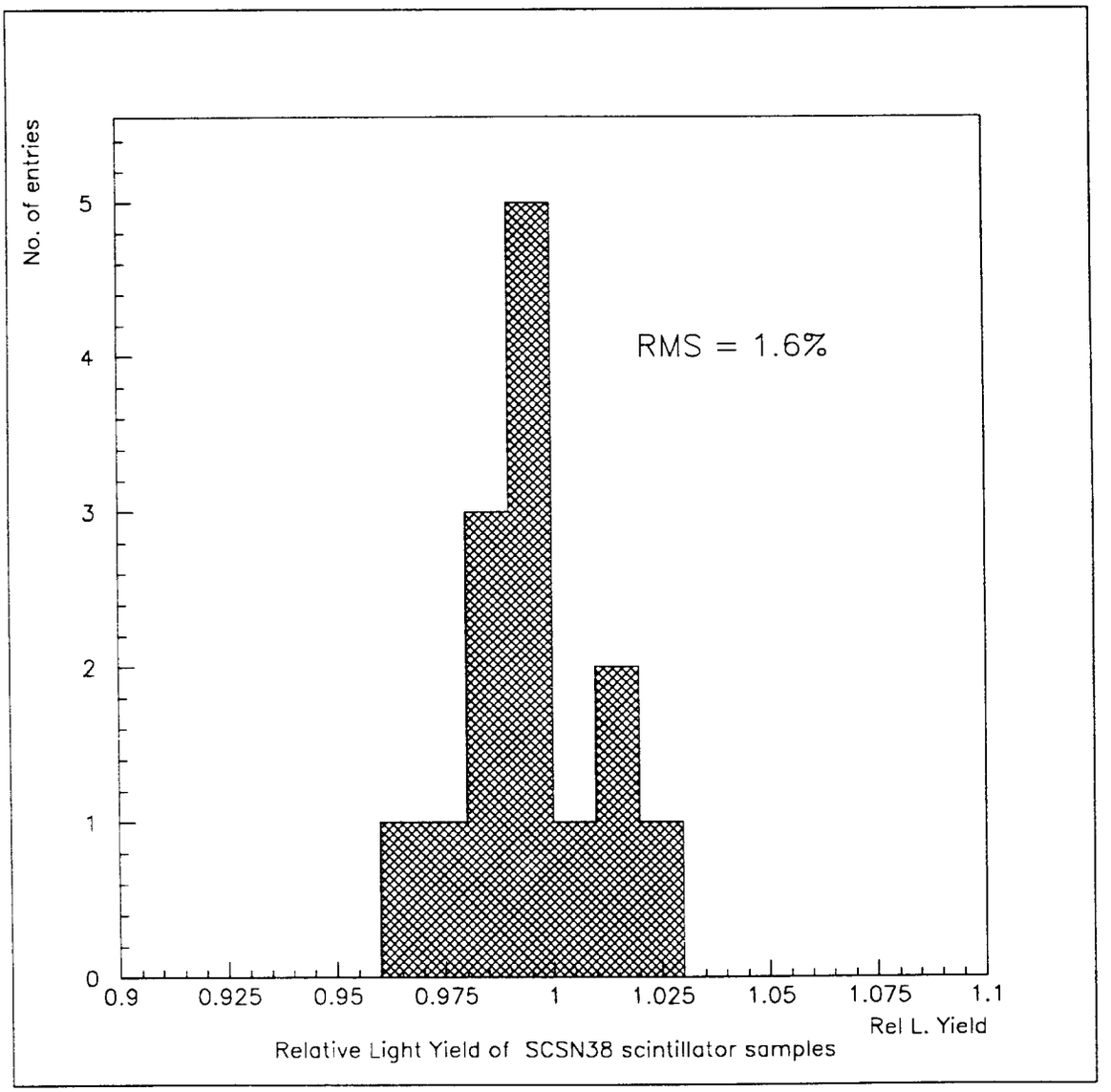

Fig. 6. The distribution of the relative light yield of a set of scintillator samples, as determined from the absorption spectrum of Bi^{207} β source. The RMS of this distribution is 1.6%.

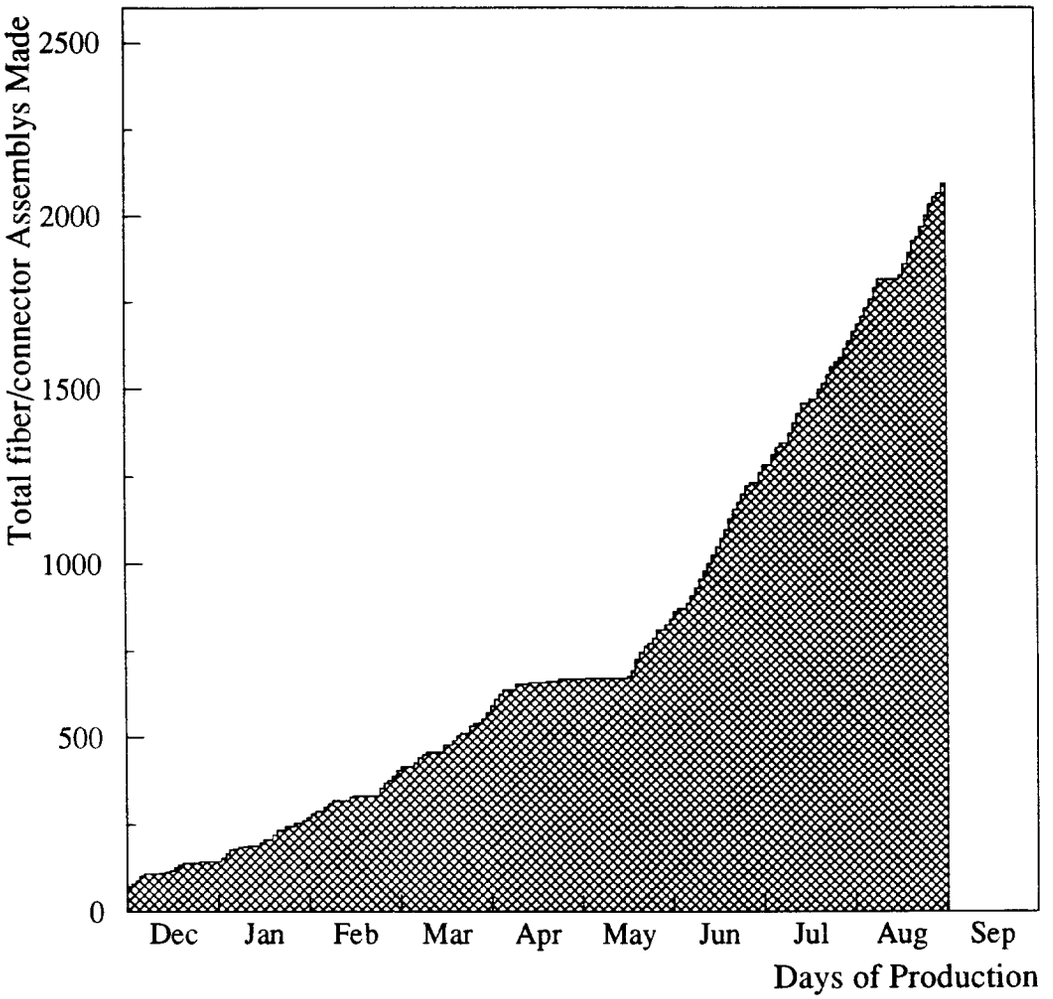

Fig. 7. The rate of production of fiber/connector assemblies.

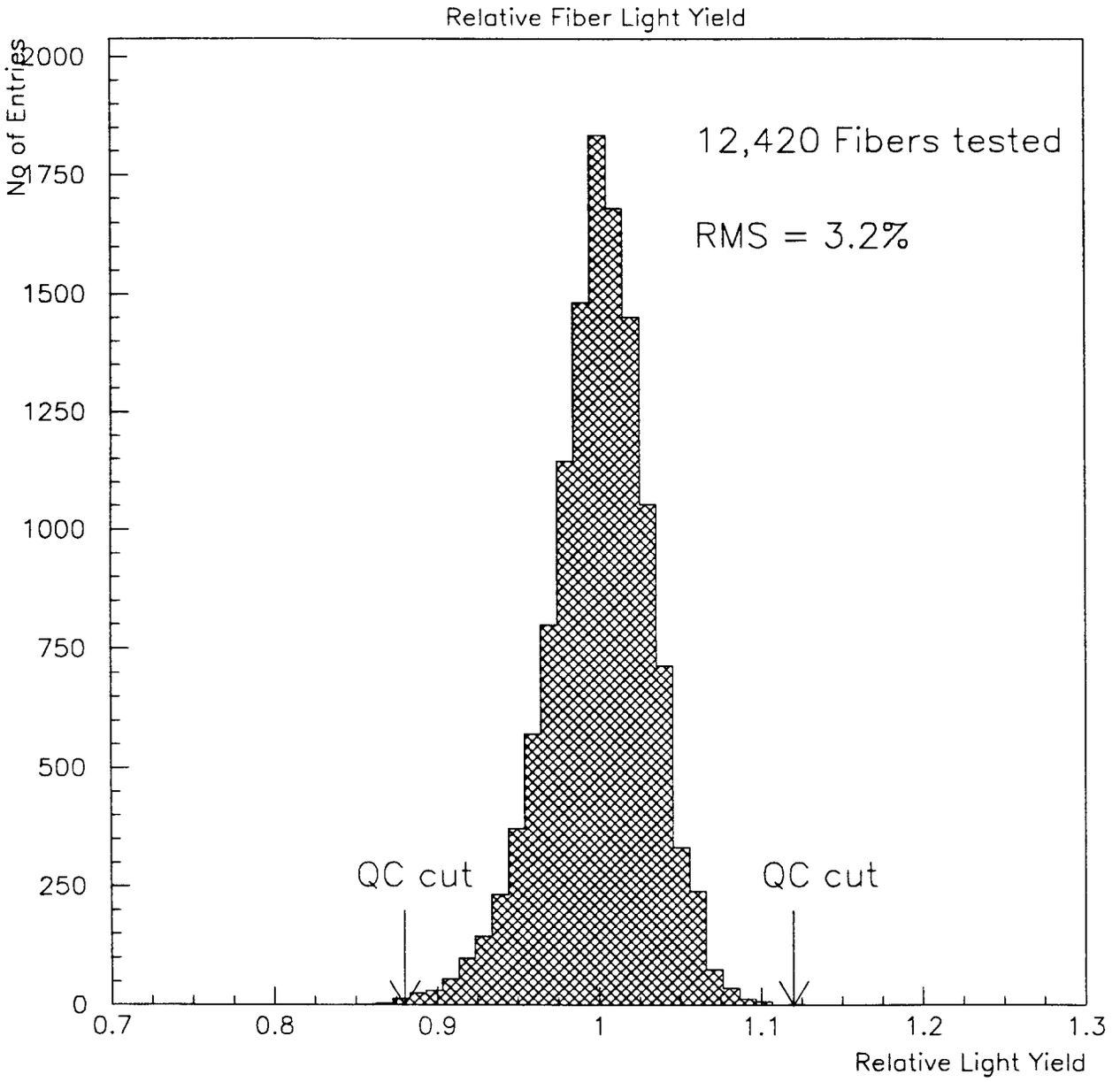

Fig. 8. Distribution of the relative light yield of the optical fibers . The RMS of the fiber light yield equals 3.2% and the nongaussian tail of the distribution may is caused by the fibers with imperfections in the cladding surface. The fibers with relative light yield of less than 12% below the average were rejected.

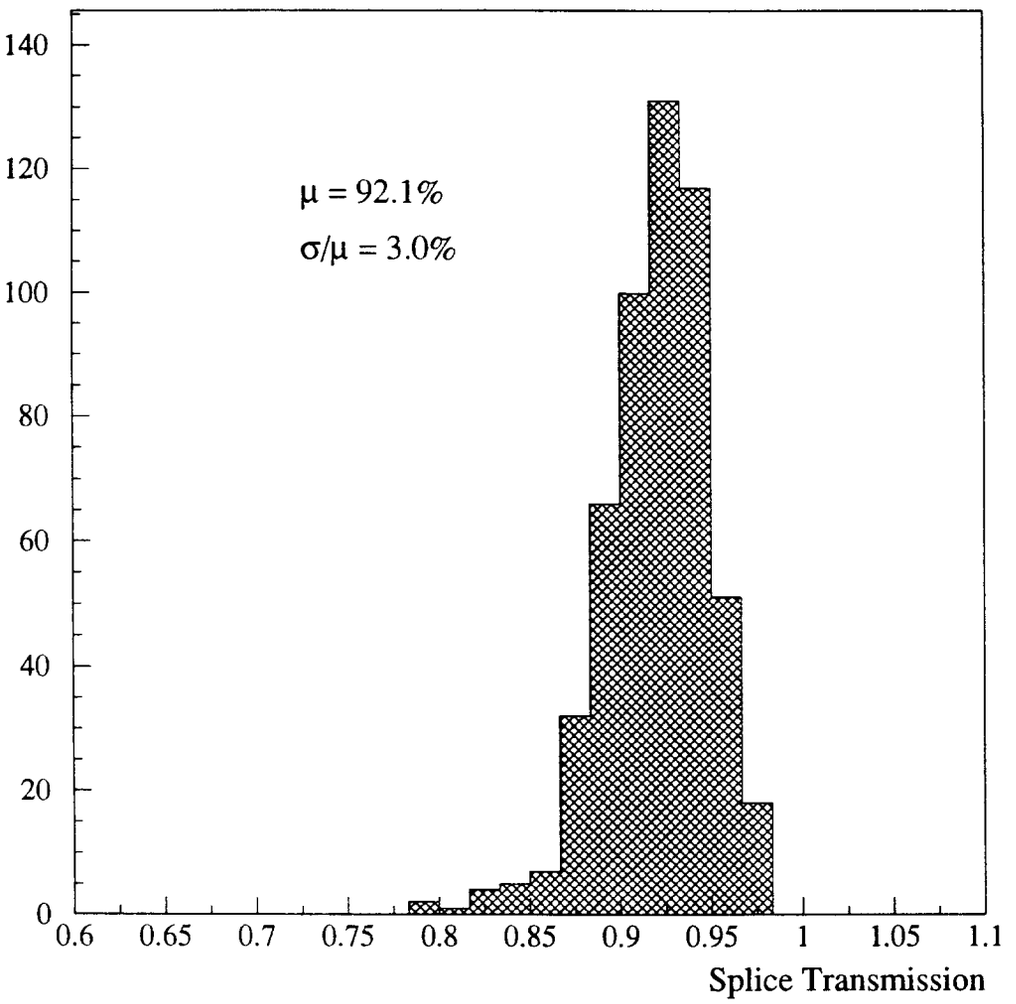

Fig. 9. Distribution of light transmission across splice between sets of two green WLS fibers.

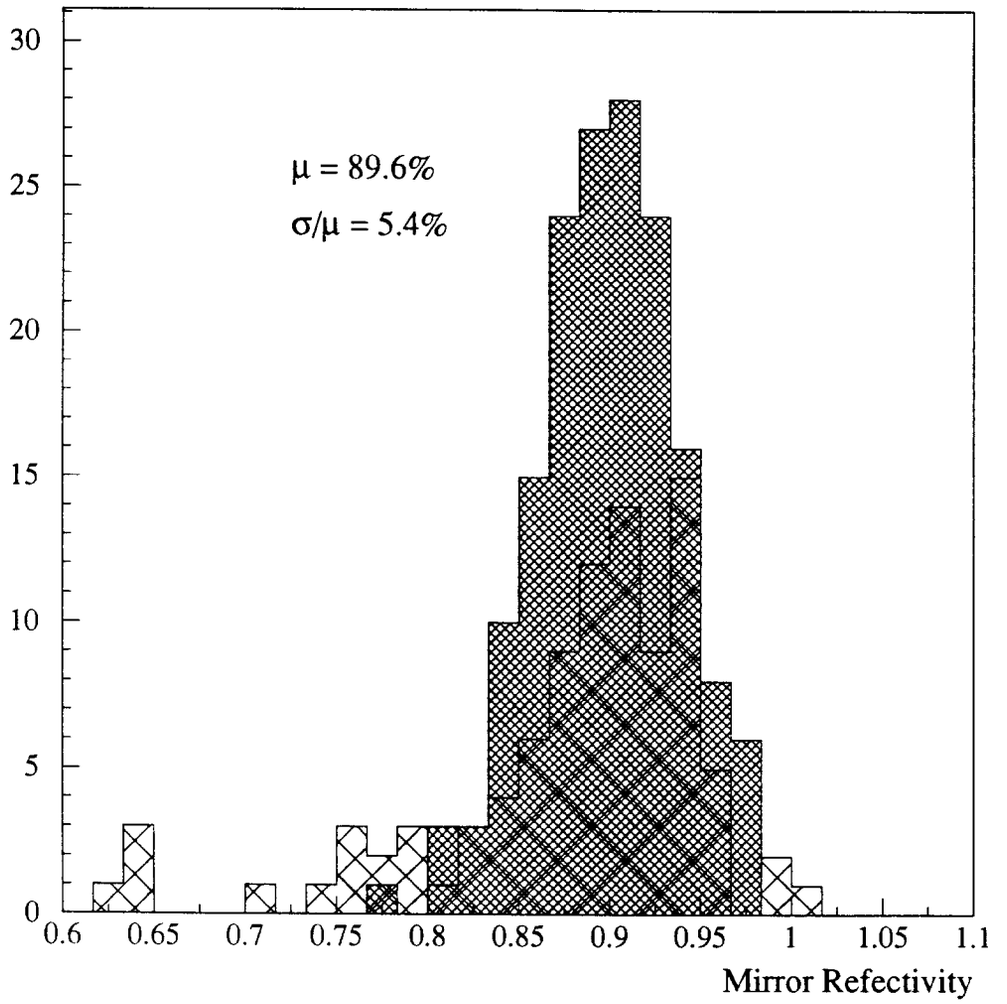

Fig. 10. Distribution of the reflectivity of mirror. The cross-hatched area corresponds to the mirror reflectivity of fibers processed during the period of malfunctioning of the sputtering machine. Fibers mirrored during that specific period were not included in the production of connector assemblies for the CDF End Plug Hadron calorimeter. The mean (μ =89.6%) and the RMS (σ/μ= 5.4%) of mirror reflectivity were calculated after the exclusion of the fibers mirrored during the period of malfunctioning of the sputtering machine.

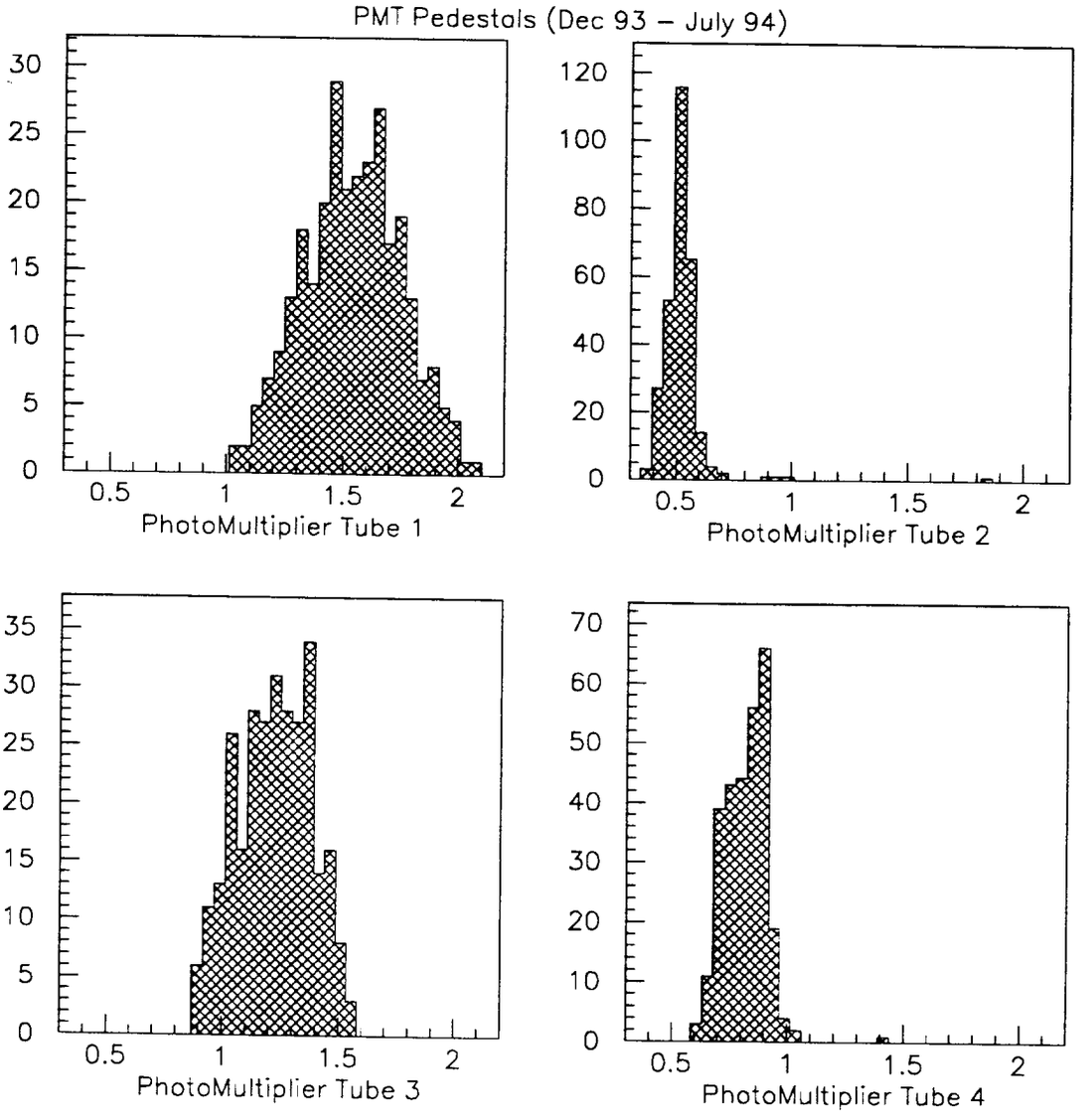

Fig. 11. The measure pedestals (dark current) of each PMT (Hamamatsu R580-17, 10 stage, green extended) in nanoamps (nA) as monitored over seven months. The RMS of each PMT pedestal is between 0.1 nA to 0.2 nA. These values are relatively small, as a typical signal from a tile exposed to the collimated source is about 50 nA.

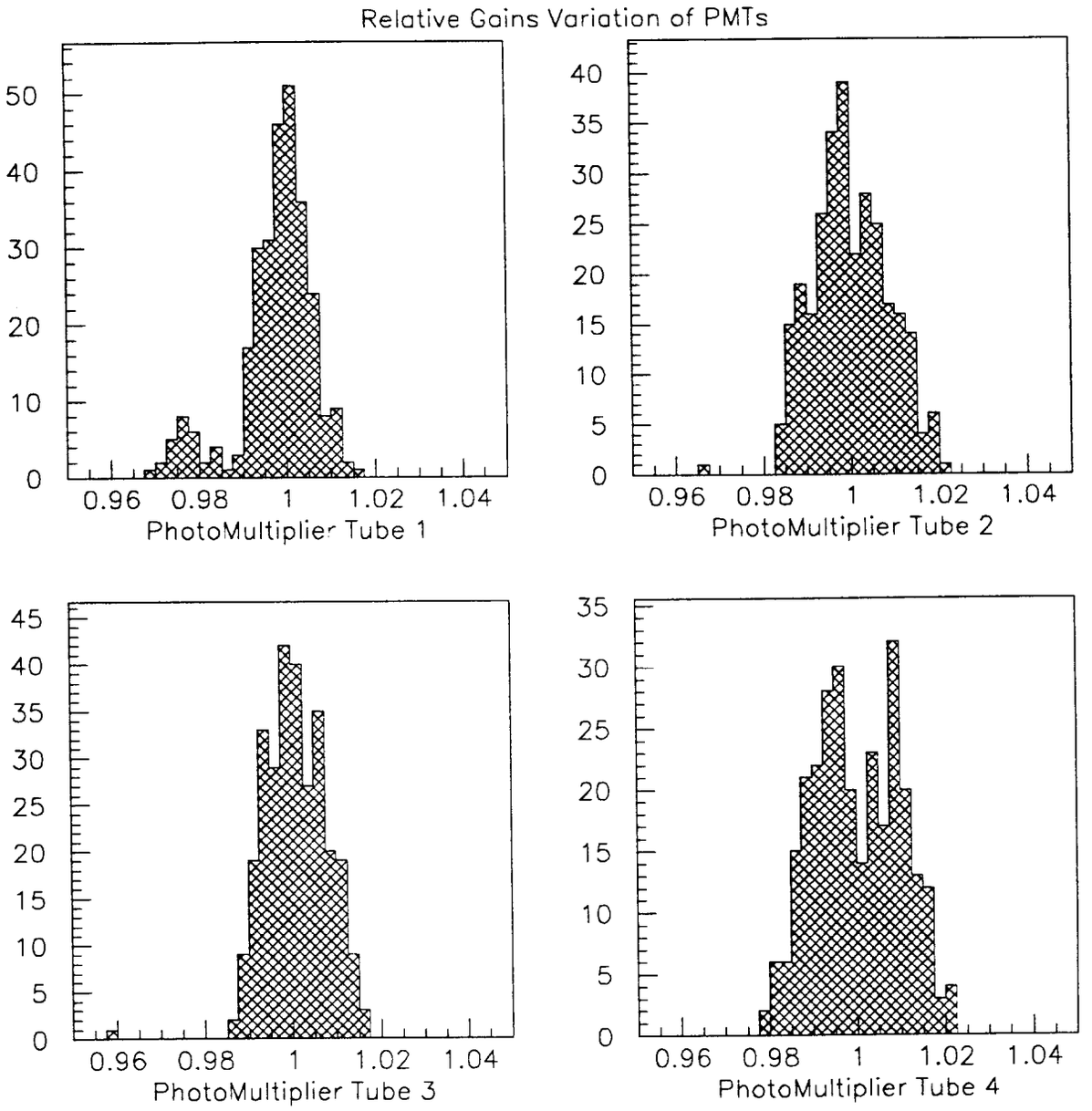

Fig. 12. The relative gain of four photomultiplier tubes used in the QC tests of megatiles. The RMS of each pmt is 0.9%, 0.9%, 0.7%, and 1.0% respectively. The PMTs were run at high voltage of $\approx$ 1350 Volts corresponding to a typical gain of 1×10^6.

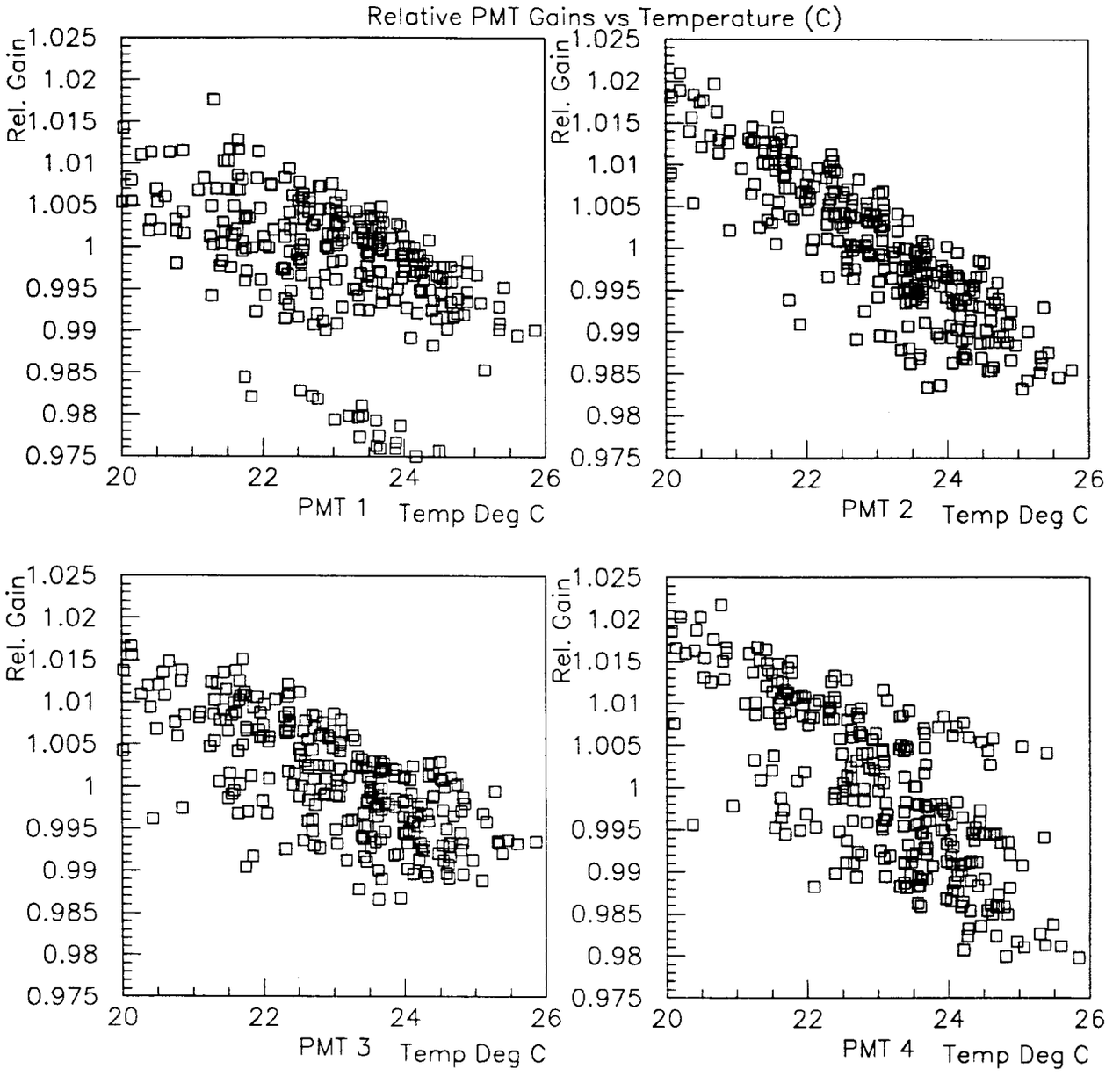

Fig. 13. The relative gain of each PMT plotted as a function of temperature in ^{o}C. There is a negative correlation between the PMT relative gain and its temperature.

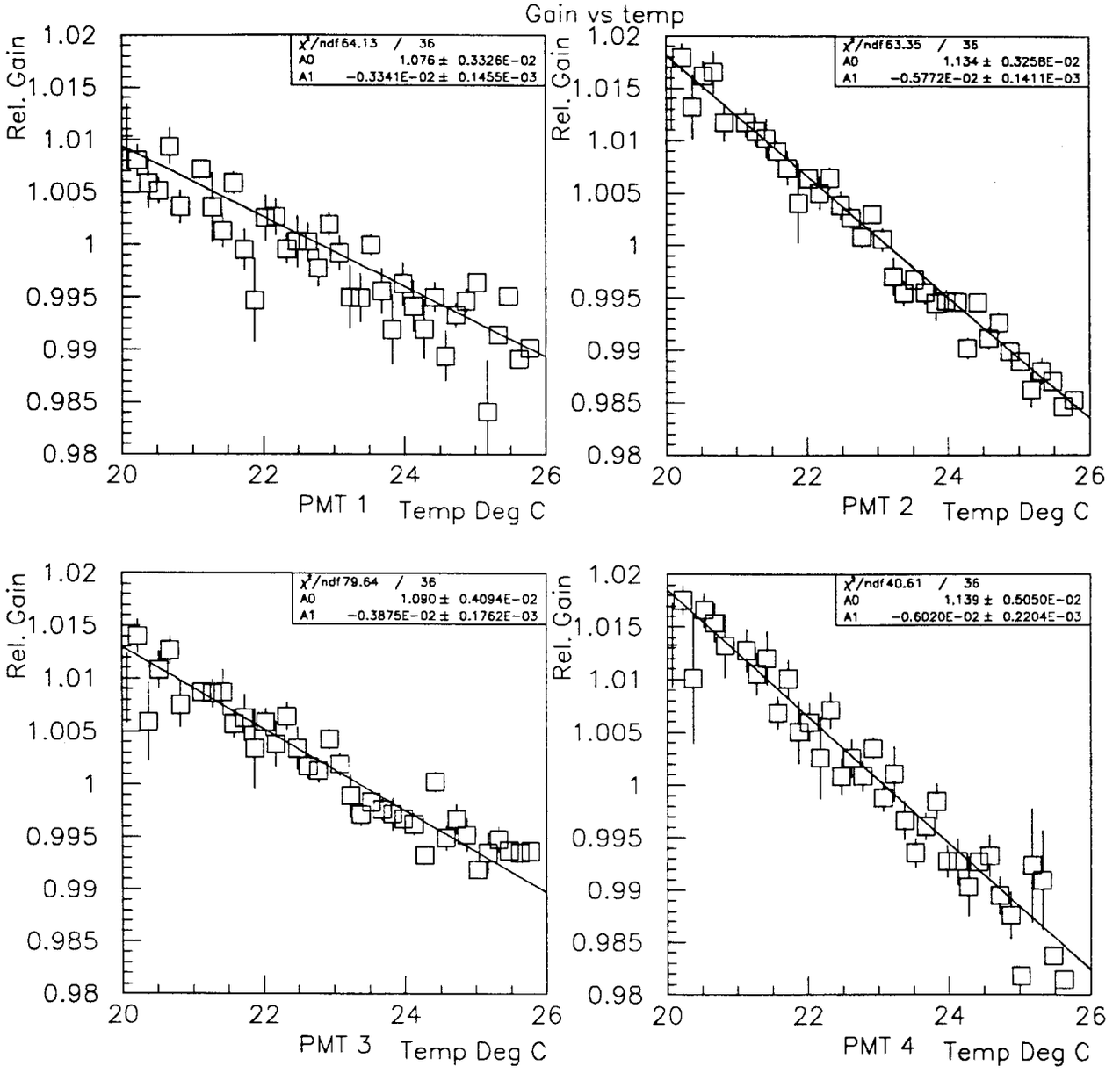

Fig. 14. The average relative gain of each PMT versus temperature. It is fitted to a first order polynomial function (ax+b). The slope corresponds to the gain temperature coefficients of -0.3%/^0C to -0.6%/^0C.

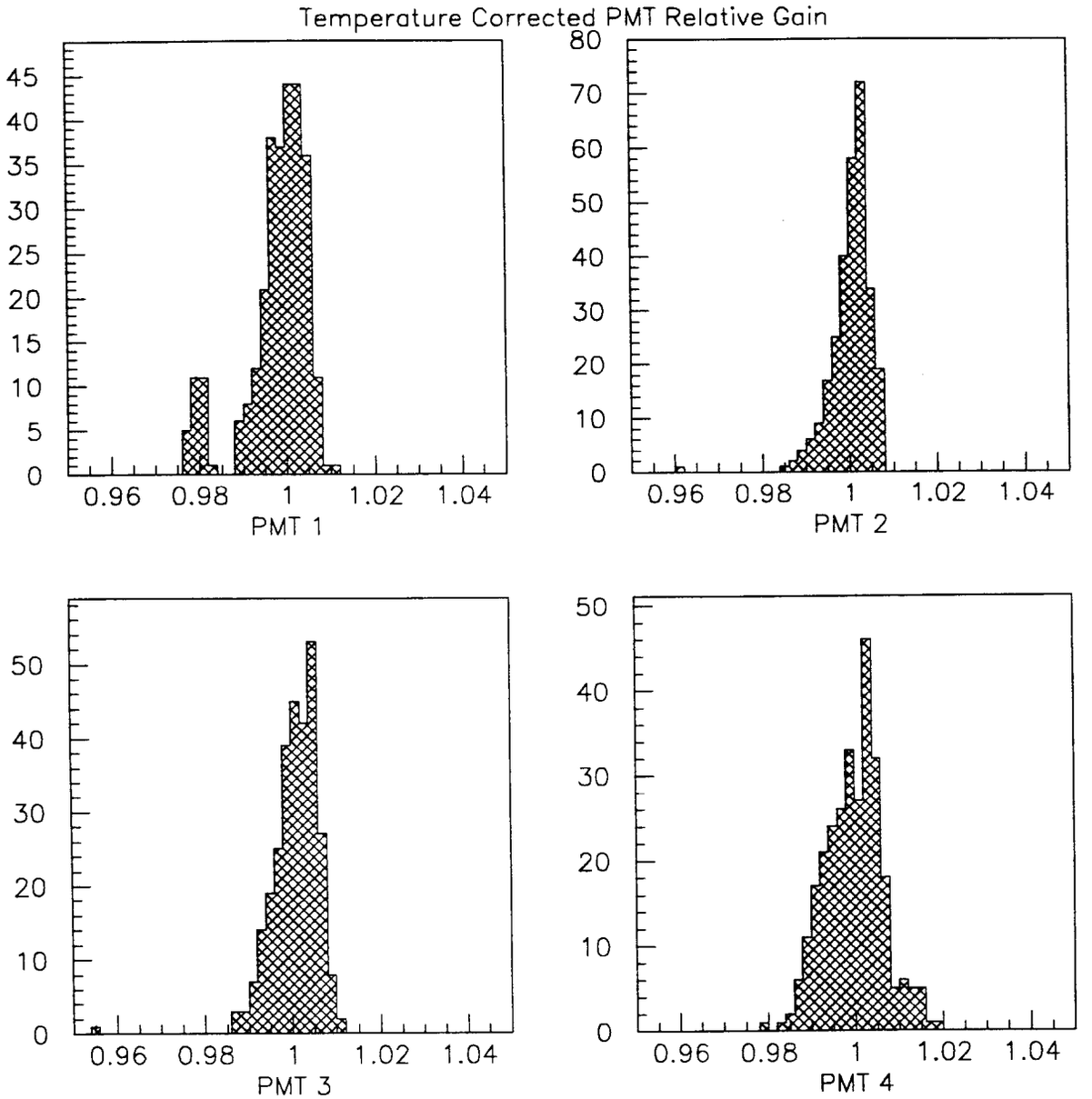

Fig. 15. The relative gain of each PMT after correcting for the temperature dependence of each PMT. The RMS of the distributions are 0.7%, 0.5%, 0.5%, 0.7% respectively. The data corresponds to the QC tests performed between Dec '93 and Aug '94.

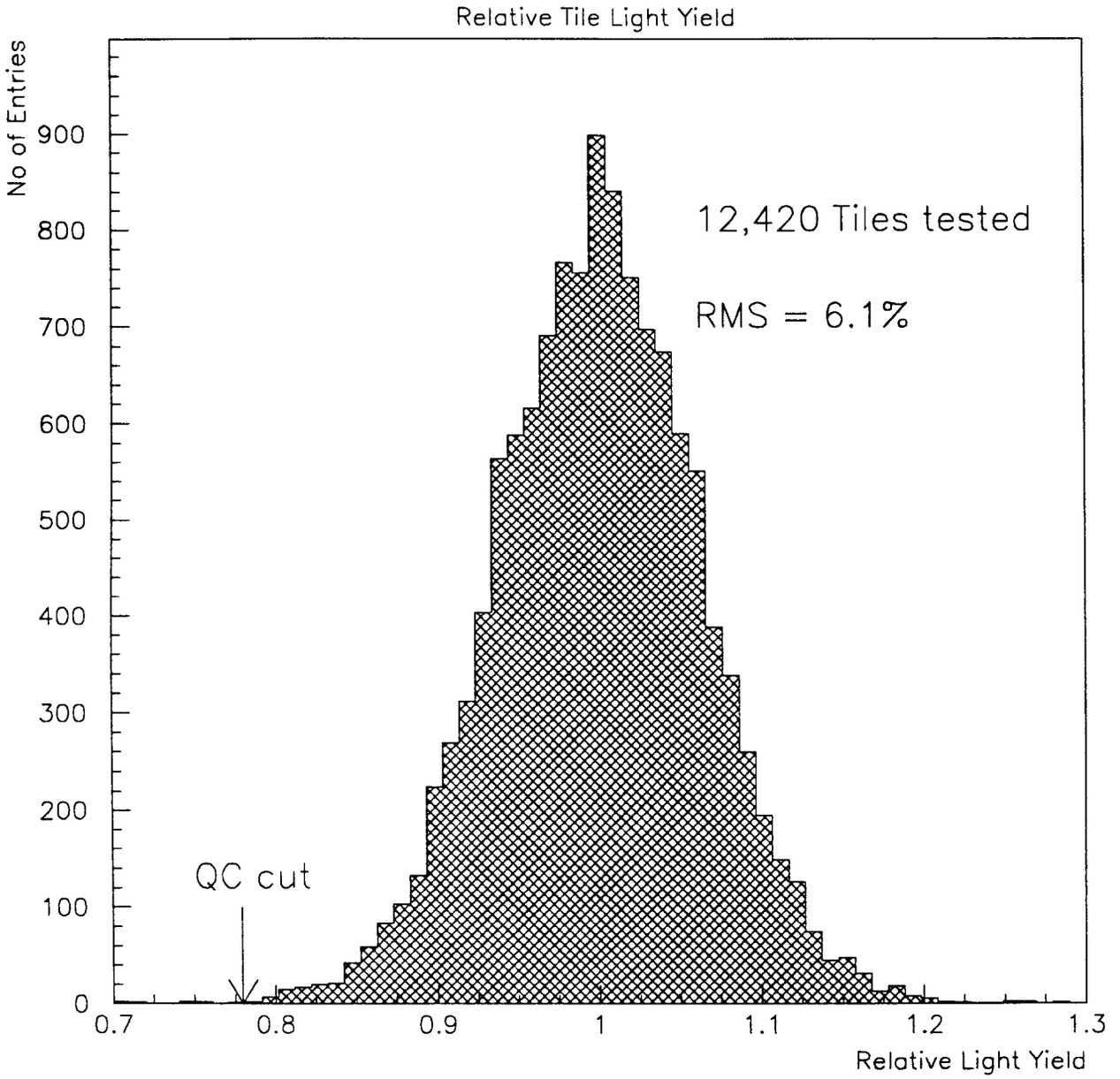

Fig. 16. The distribution of the relative tile light yield for the collimated γ source. The RMS of the tile light yield is 6.1%. The tiles with relative light yield 22% or less below the average would fail QC test. In such a case, the fiber used to read out particular tile was replaced and entire megatile was re-tested.

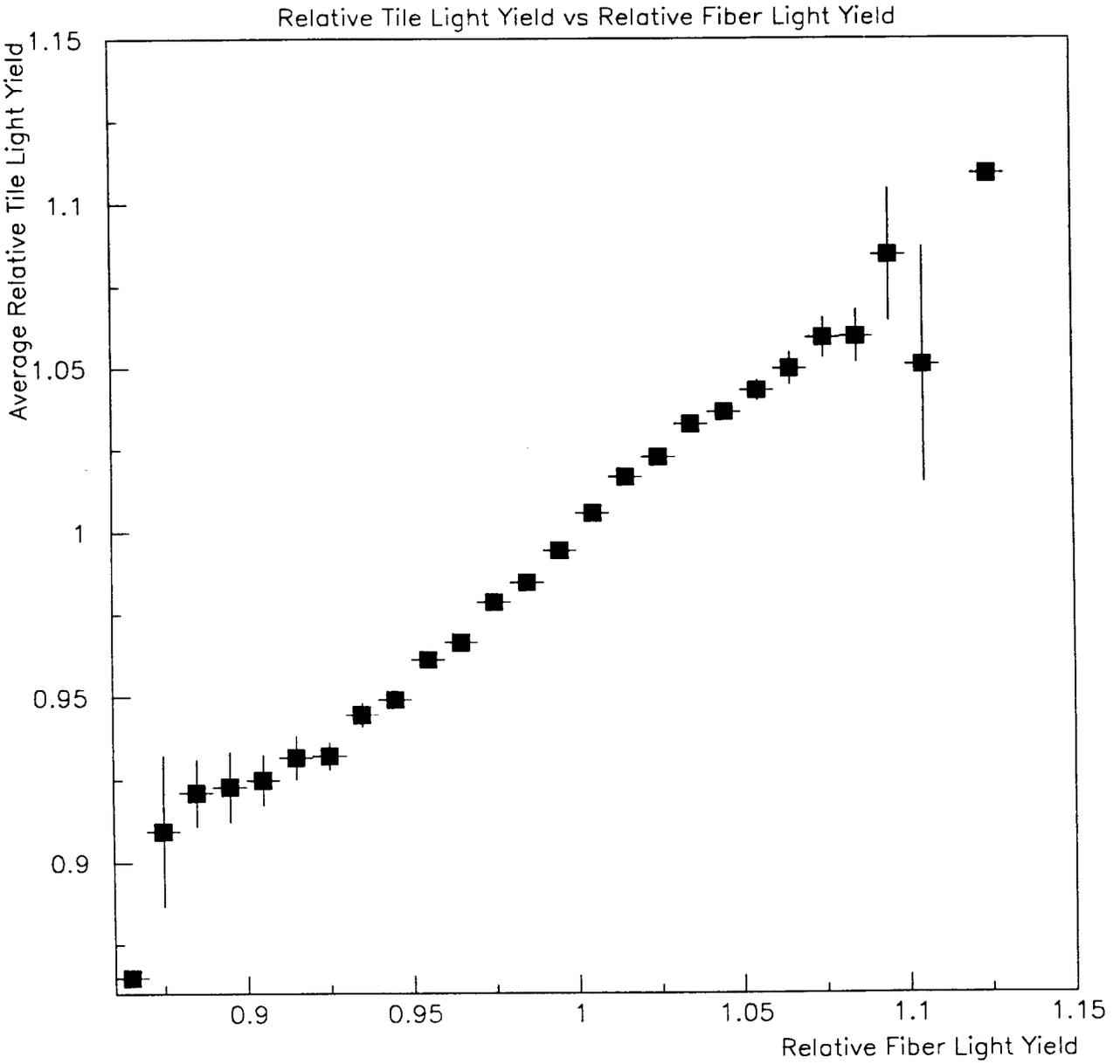

Fig. 17. The correlation between the collimated γ source tile light yield and the fiber light yield mean using the UV scanner. Each vertical error bar shows the uncertainty in the mean of the tile light yield for that particular binning value of the fiber light yield. Since the RMS of fiber light yield is 3.2%, most of the fibers populate the region of relative light yield between 0.95 and 1.05 on the horizontal axis of the plot.

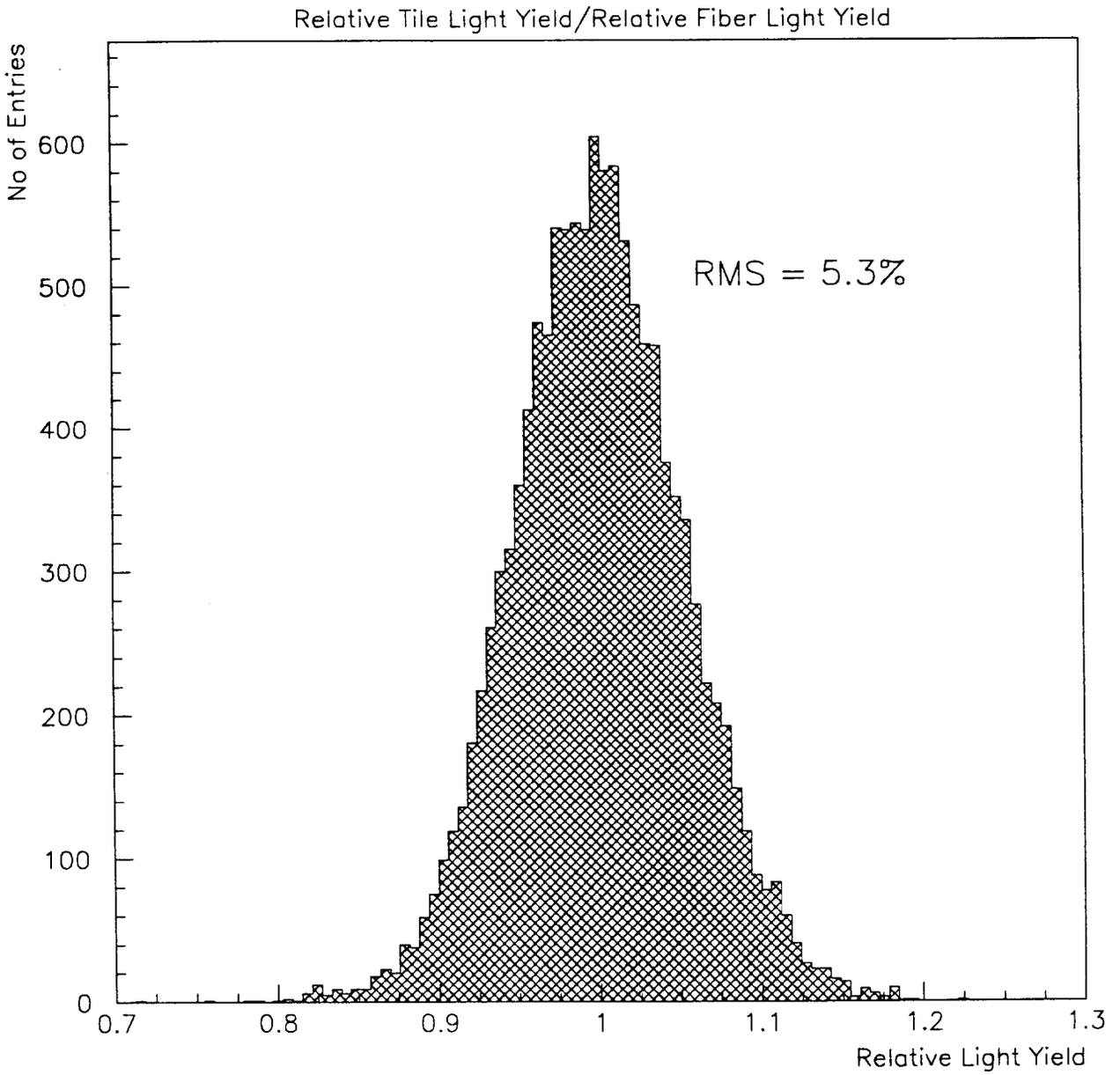

Fig. 18. Distribution of the relative tile light yield (as measured using the collimated γ source) divided by its fiber light yield (as measured using the UV setup, see Fig. 8). The RMS of this distribution is 5.3%.

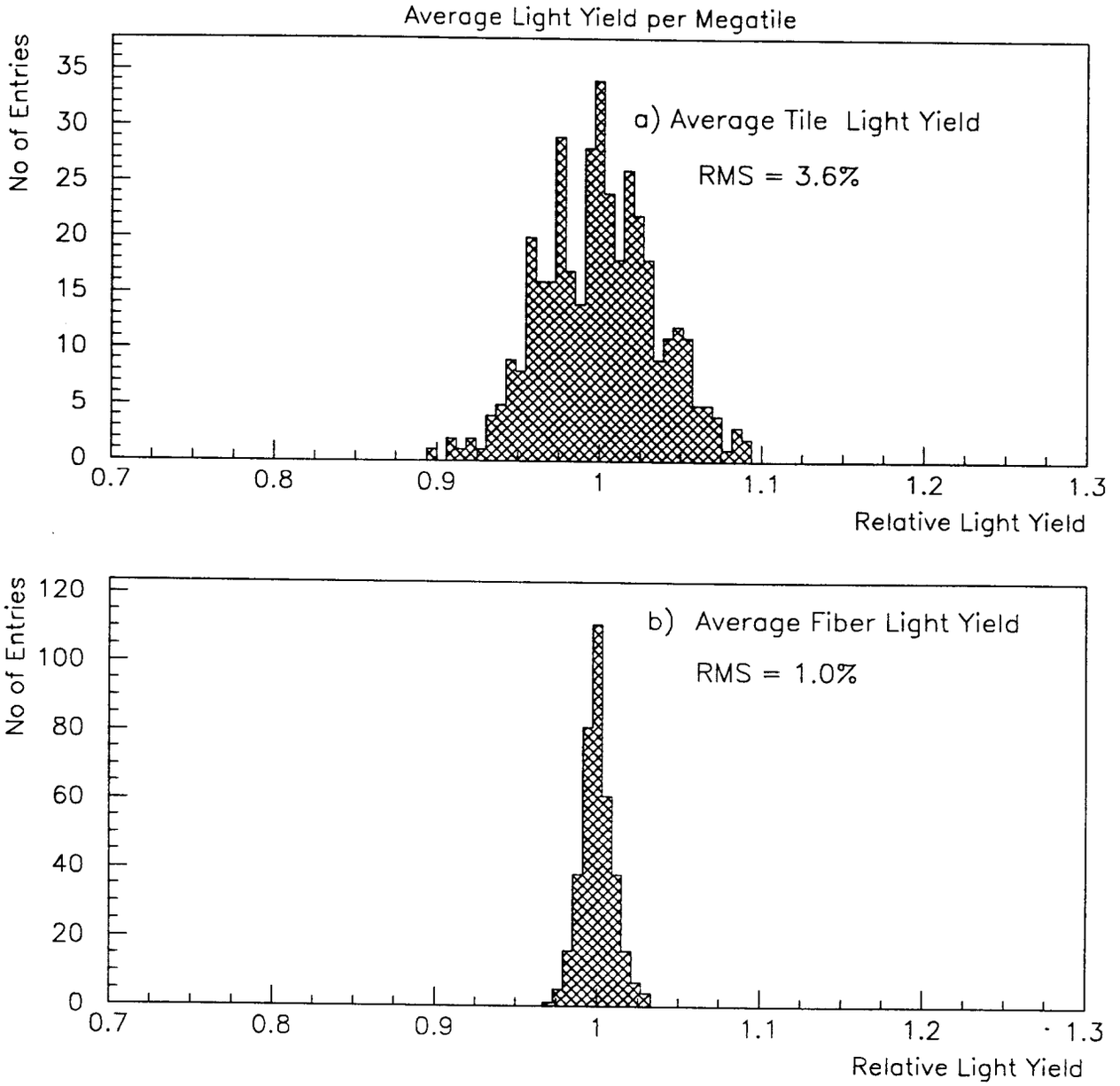

Fig. 19. a) Distribution of the average megatile light yield, defined as the average relative light yield of all the tiles from a particular megatile. The RMS of this distribution is 3.6%. b) Distribution of the average fiber light yield, defined as the average relative fiber light yield of all the fibers from a particular megatile. The RMS of this distribution is 1.0%

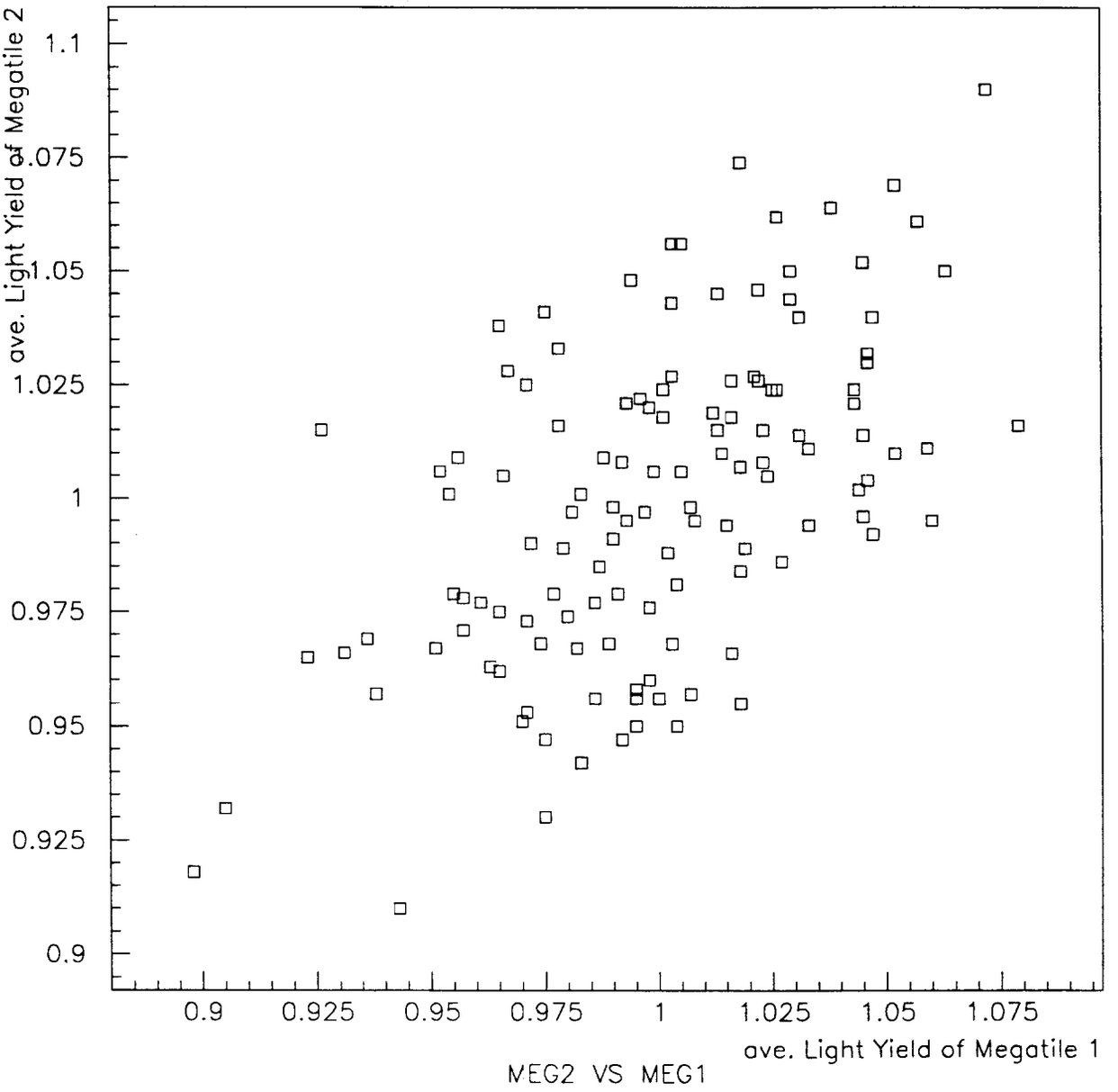

Fig. 20. Scatter plot of average megatile light yield for pairs of megatiles cut from same scintillator sheets. The correlation between the average light yields of two megatiles cut from the same scintillator sheet indicates that indeed one of the production processes taking place in Lab 8 (cutting of fiber grooves, painting the tiles edges with white paint and filling the separation grooves with white paint/epoxy mixture) contributed to the variation of the average megatile light yield.

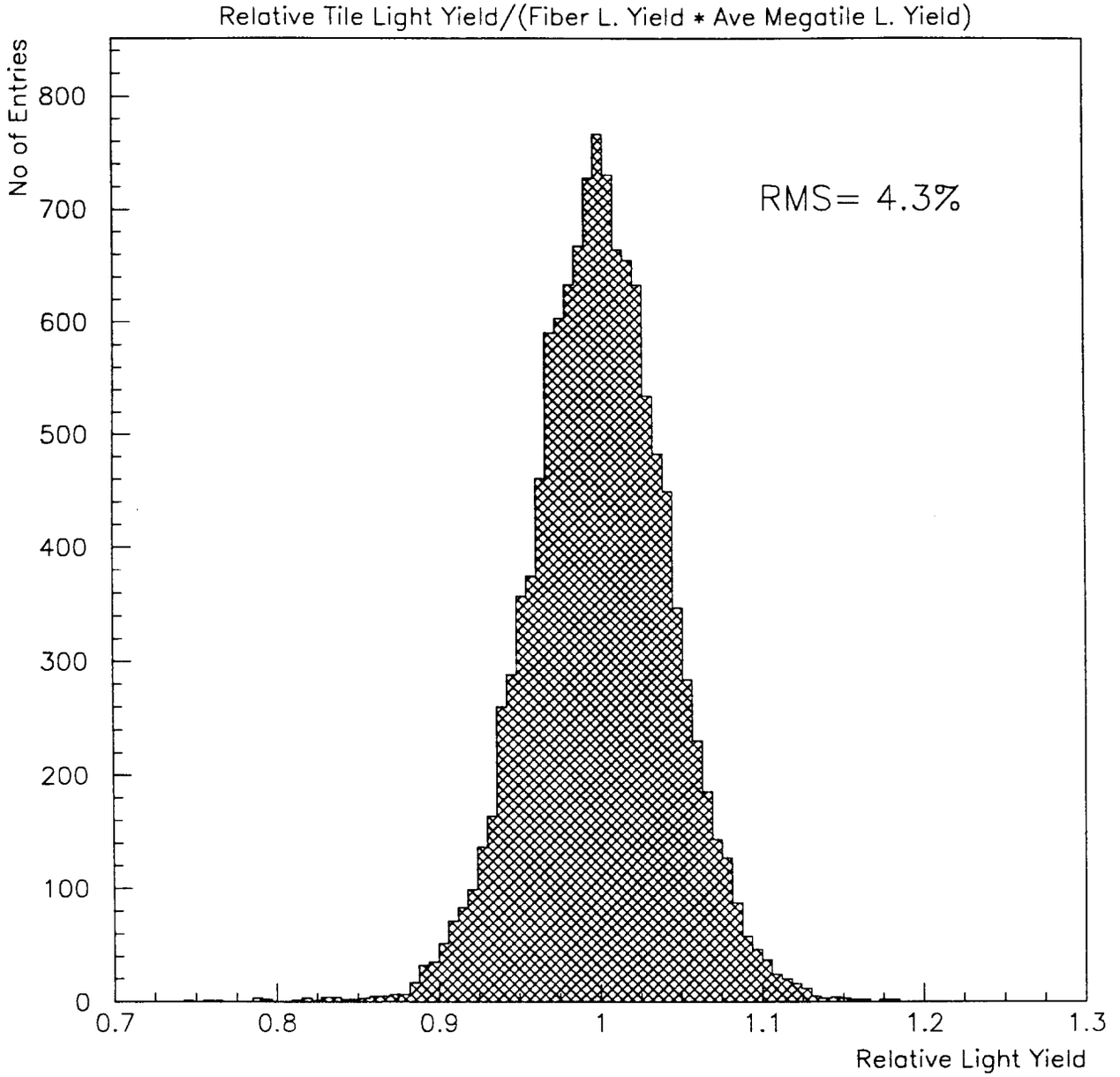

Fig. 21. Distribution of the relative tile light yield divided by both the relative fiber light yield of the corresponding tile (see Fig. 8) and the average collimated γ source tile light yield of the corresponding megatile (see Fig. 19). The RMS is 4.3%.

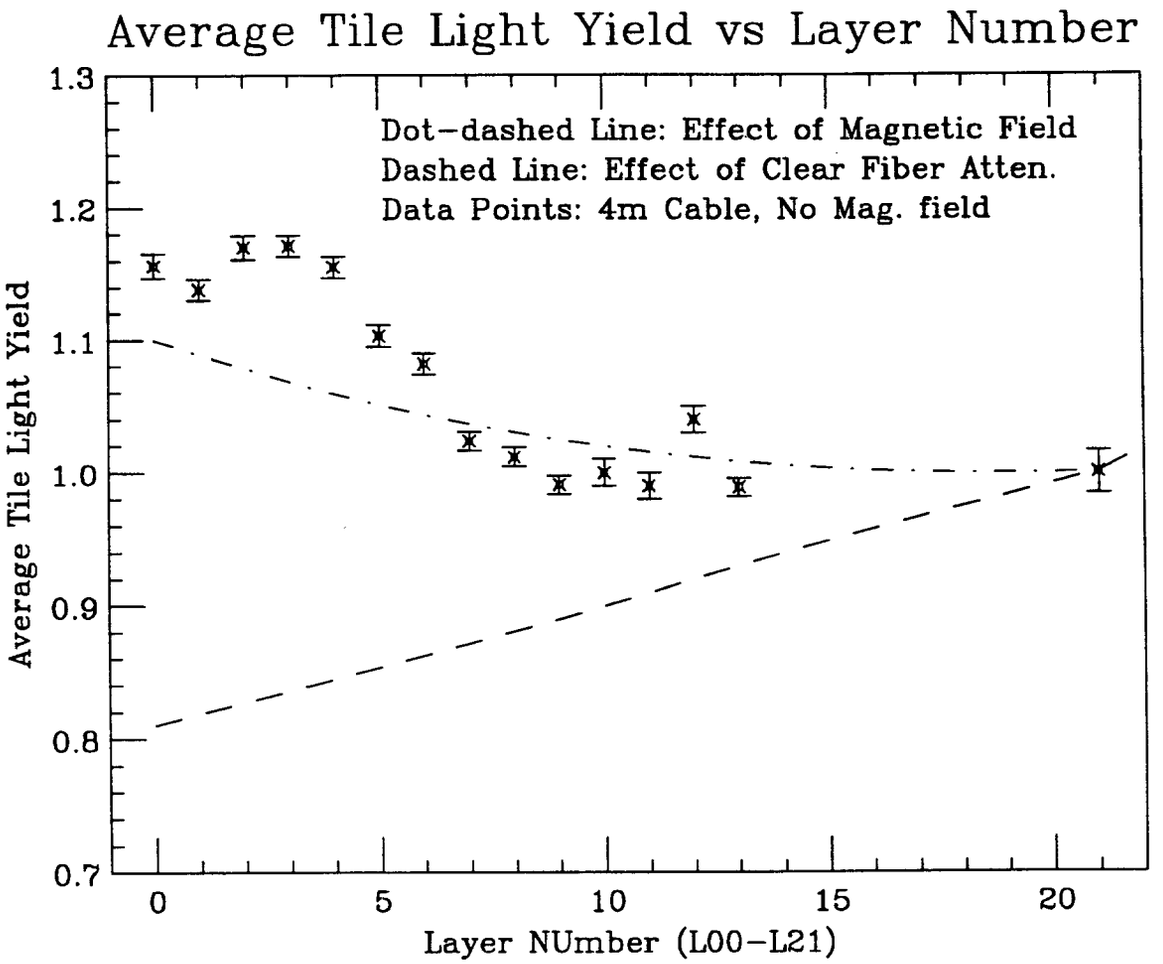

Fig. 22. The average tile light yield plotted as a function of megatile layer number. At the design stage, the average light yield of tiles was adjusted by varying the length of green WLS fibers inside tiles, as well as by a suitable choice of the distance between the tiles edge and the position of WLS-to-clear fiber splice. The light yield of tiles were normalized to the light yield of the subset of L21 and L20 megatiles. The plot indicates an approximately 10% increase in the average light yield of inner most sampling layers of the hadron calorimeter. Dashed and dot-dashed lines indicate the effects of attenuation length of clear optical readout cables and magnetic field respectively, on the final light yield of tiles.

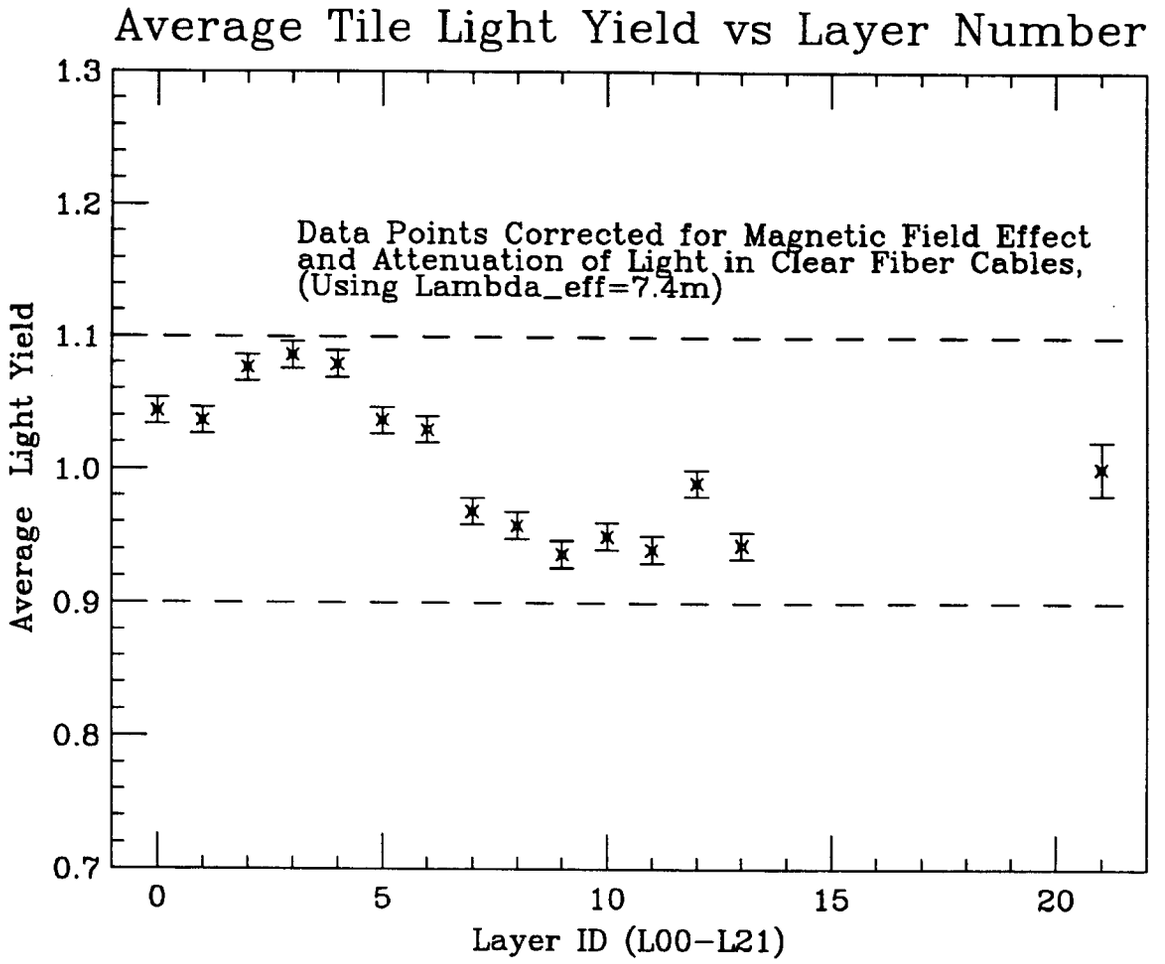

Fig. 23. The relative tile light yield versus the megatile's layer number. The data points were corrected for the effects of the magnetic field and attenuation length of the clear optical readout cable. The dashed lines at ± 10% around unity indicate the design goal for the variation of the average light yield of tiles.

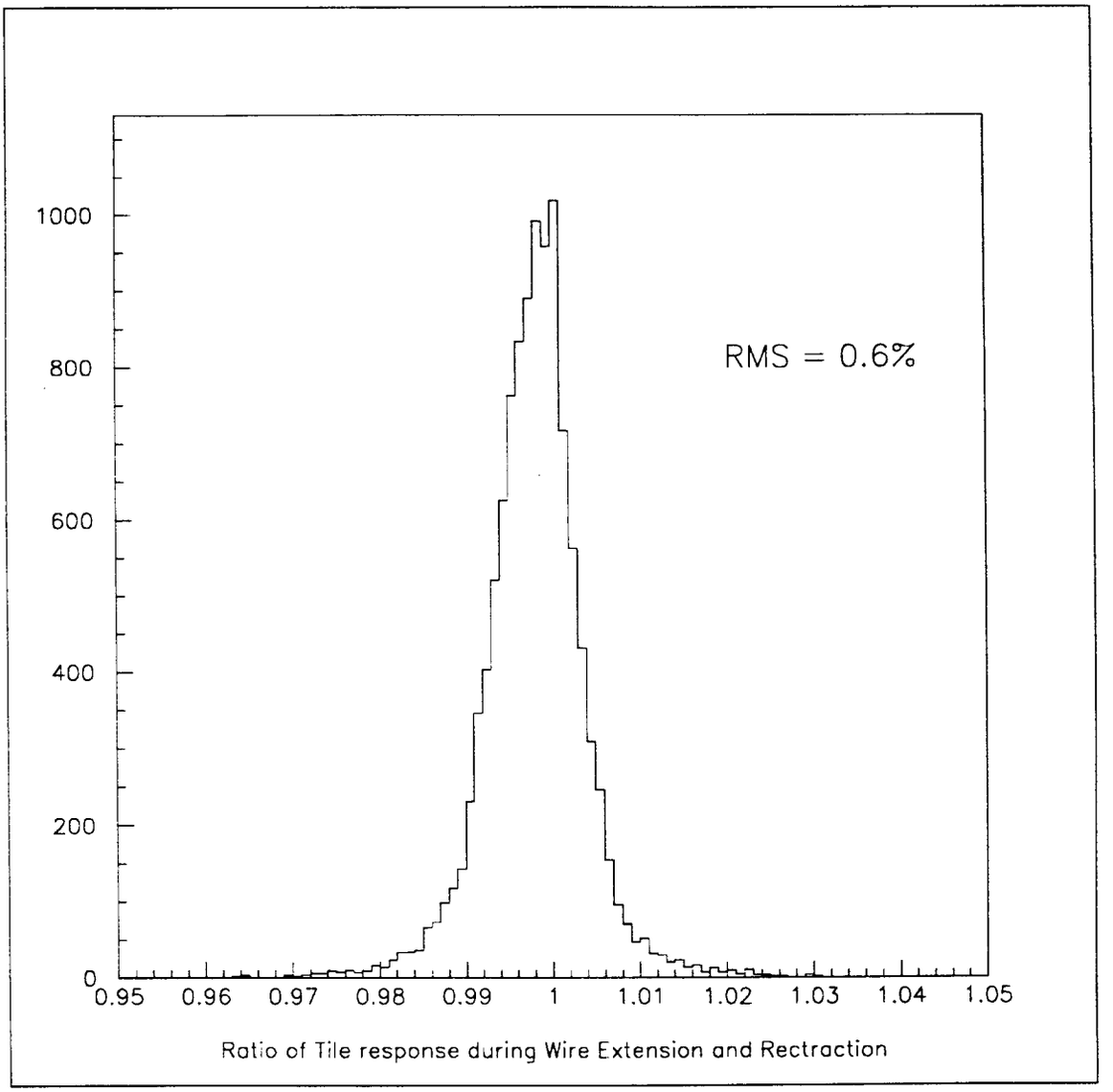

Fig. 24. Ratio of tile response to the uncollimated γ source during the wire extensions and retractions. The RMS of this distribution is 0.6%.

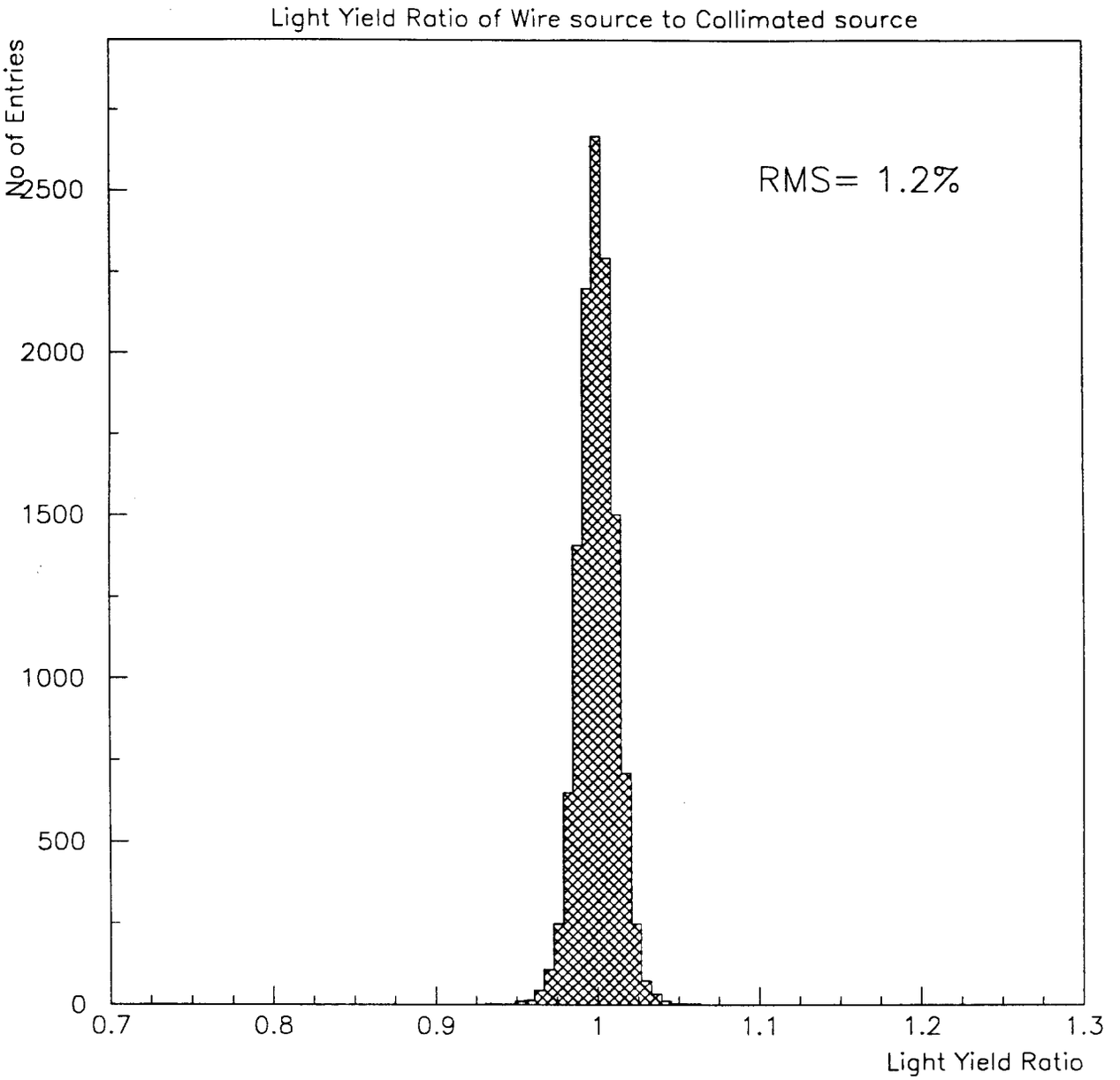

Fig. 25. Distribution of the ratio of normalized wire source to the collimated γ source tile light yield, $R^{rel}_{w/c}$. The RMS of this distribution is 1.2%.

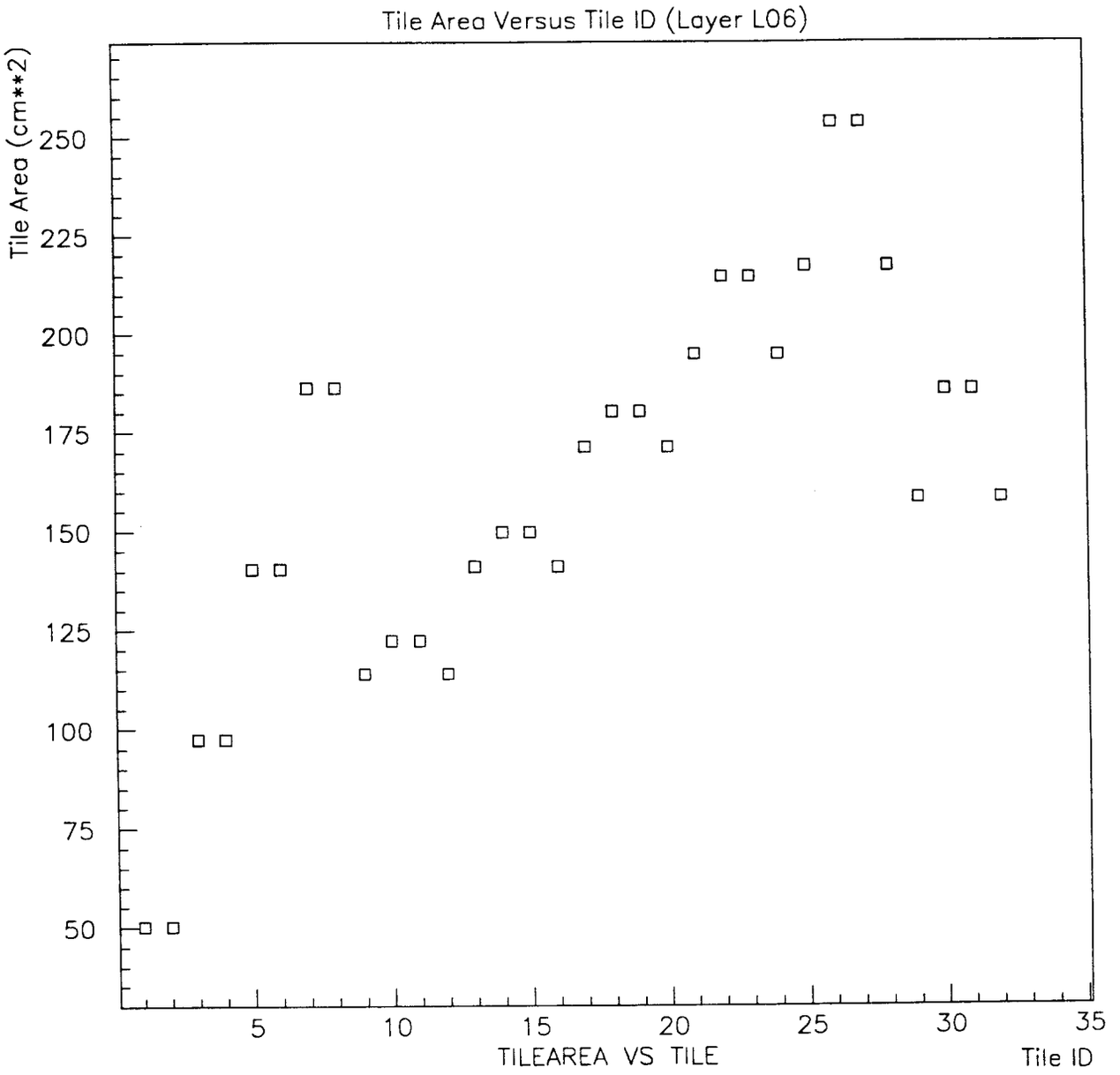

Fig. 26. The area of tiles (cm^2) versus their *Tile ID* for layer L06 megatiles, as assigned on Fig. 3. The first eight tiles have 15^0 ϕ segmentation, while tiles 9 through 32 have 7.5^0 ϕ segmentation. Tiles 29 through 32 are smaller due to the reduced η segmentation of the plug calorimeter in this region.

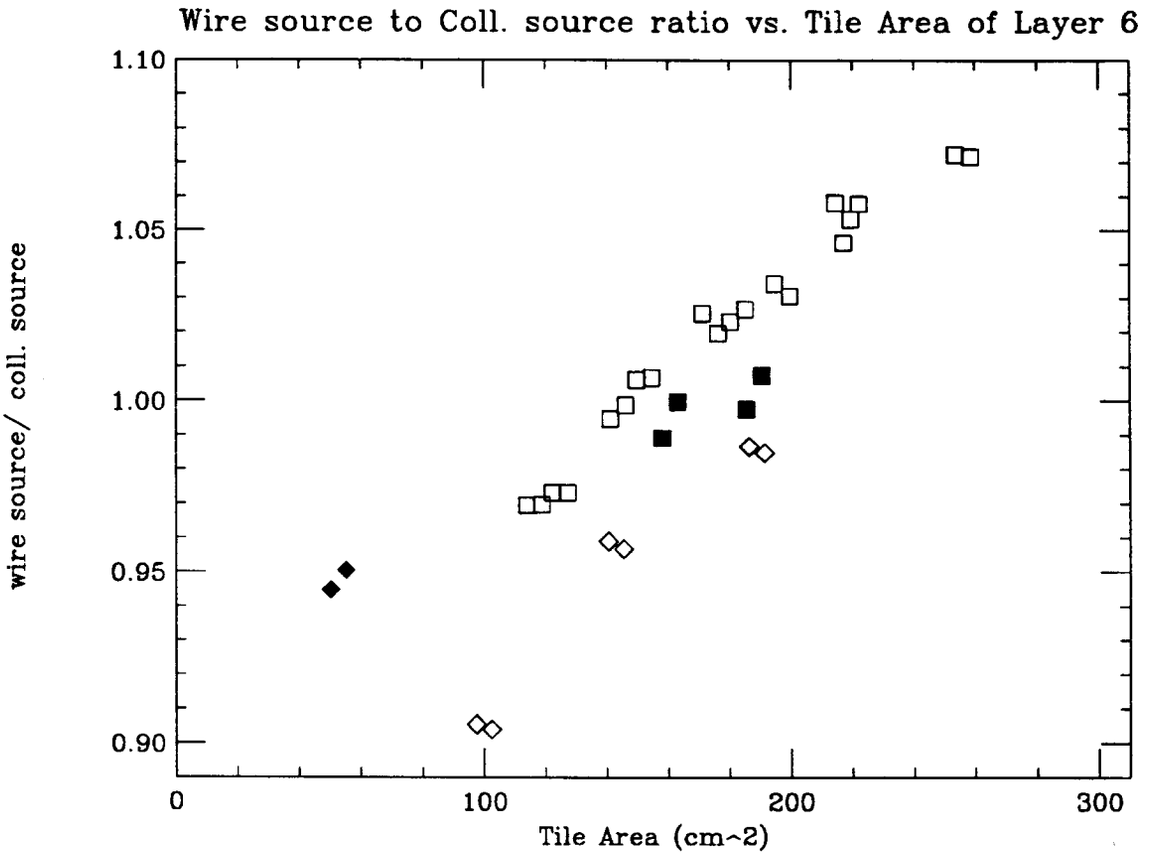

Fig. 27. Ratio $R_{w/c}^{raw}$ for layer L06. The ratio of wire source to collimated source increases as a function of the size of the tiles. The diamond symbols correspond to the tiles with 15^0 ϕ segmentation (tiles 1 through 8 on Fig. 26), while the square symbols correspond to the tiles with 7.5^0 ϕ segmentation (tiles 9 through 32). The dark square symbols correspond to the four lowest η tiles with the reduced η segmentation (tiles 29 through 32). The dark diamond symbols correspond to the two highest η tiles (tiles 1 and 2), which were read out with the non-standard fiber groove shape (the J-shape instead of the σ-shape used for the other tiles).

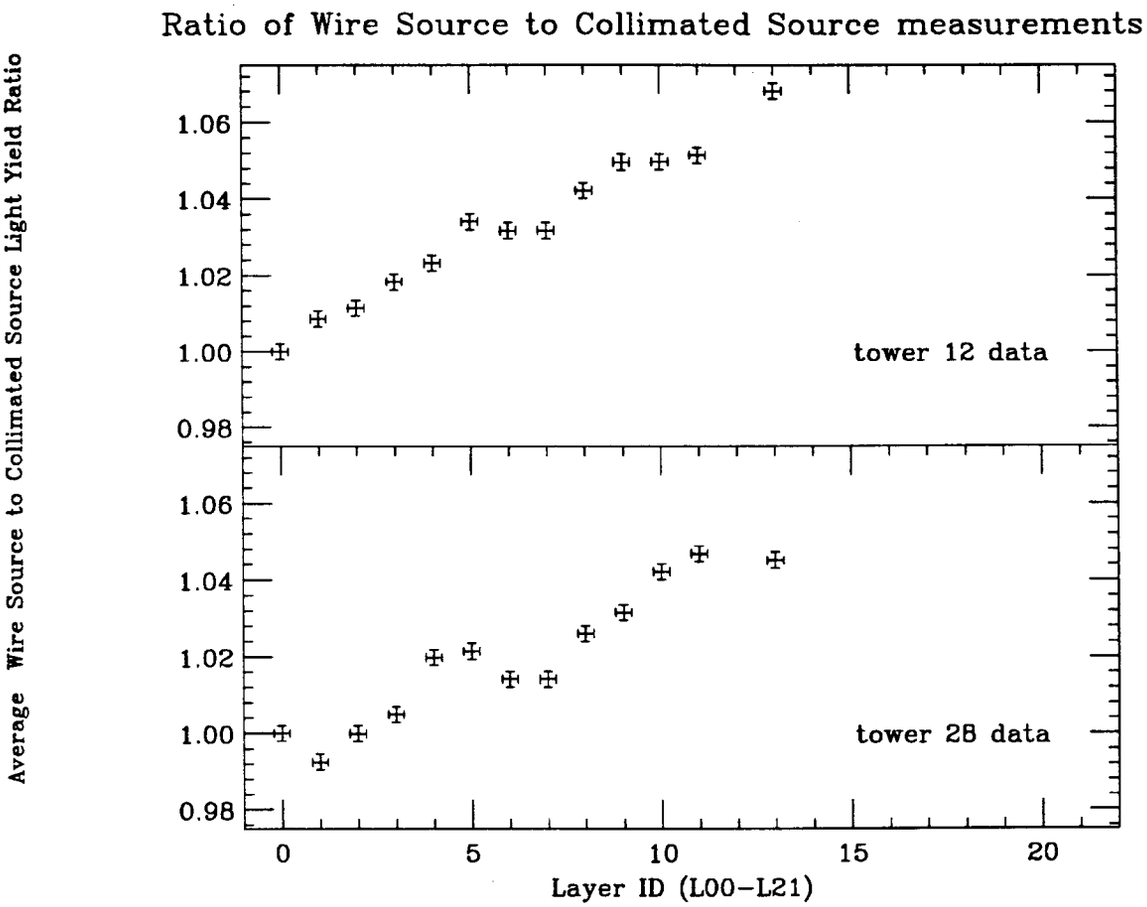

Fig. 28. Average wire to collimated source light yield ratio, normalized to the ratio for layer L00, plotted as a function of layer number. The ratio is shown for towers 12 and 28 separately.

line, ≈ 2 mm wide, applied below the separation groove. The vertical dashed line indicates the average thickness of the uncut material in the separation grooves of the Hadron megatiles.

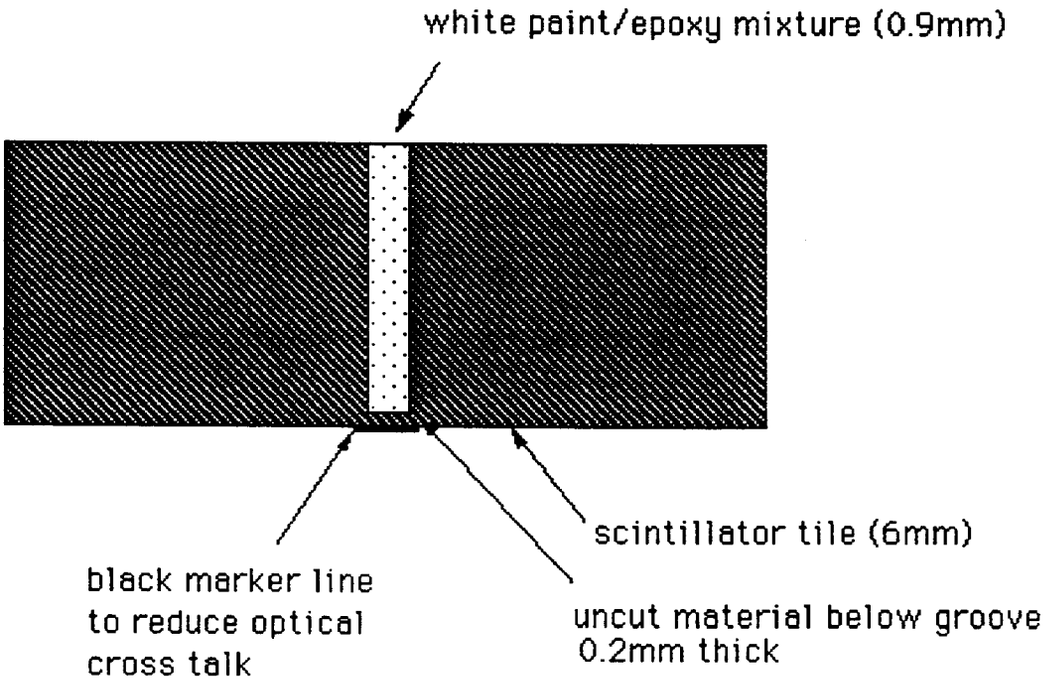

Fig. 29. The cross-sectional view of the separation groove between two tiles. The black marker line applied below the separation groove, $\approx$ 2 mm wide, reduced the optical cross-talk between the neighbouring tiles to approximately 1%.

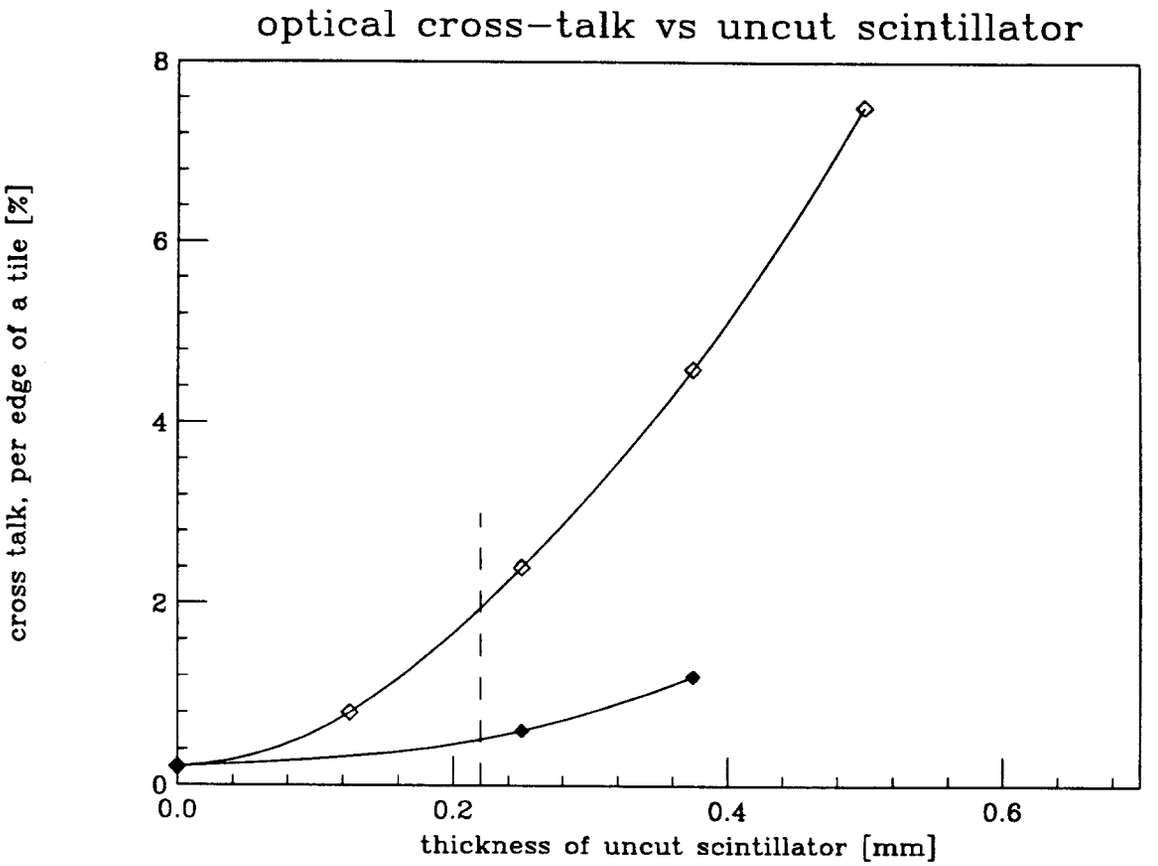

Fig. 30. R&D study of optical cross-talk between neighboring tiles as a function of uncut scintillator below the separation groove. The total thickness of the scintillator was 6 mm. The open symbols indicate the cross-talk for the case without black line applied below the separation groove. The black symbols indicate the optical cross-talk for the tiles with black line, $\approx$ 2 mm wide, applied below the separation groove. The vertical dashed line indicates the average thickness of the uncut material in the separation grooves of the Hadron megatiles.

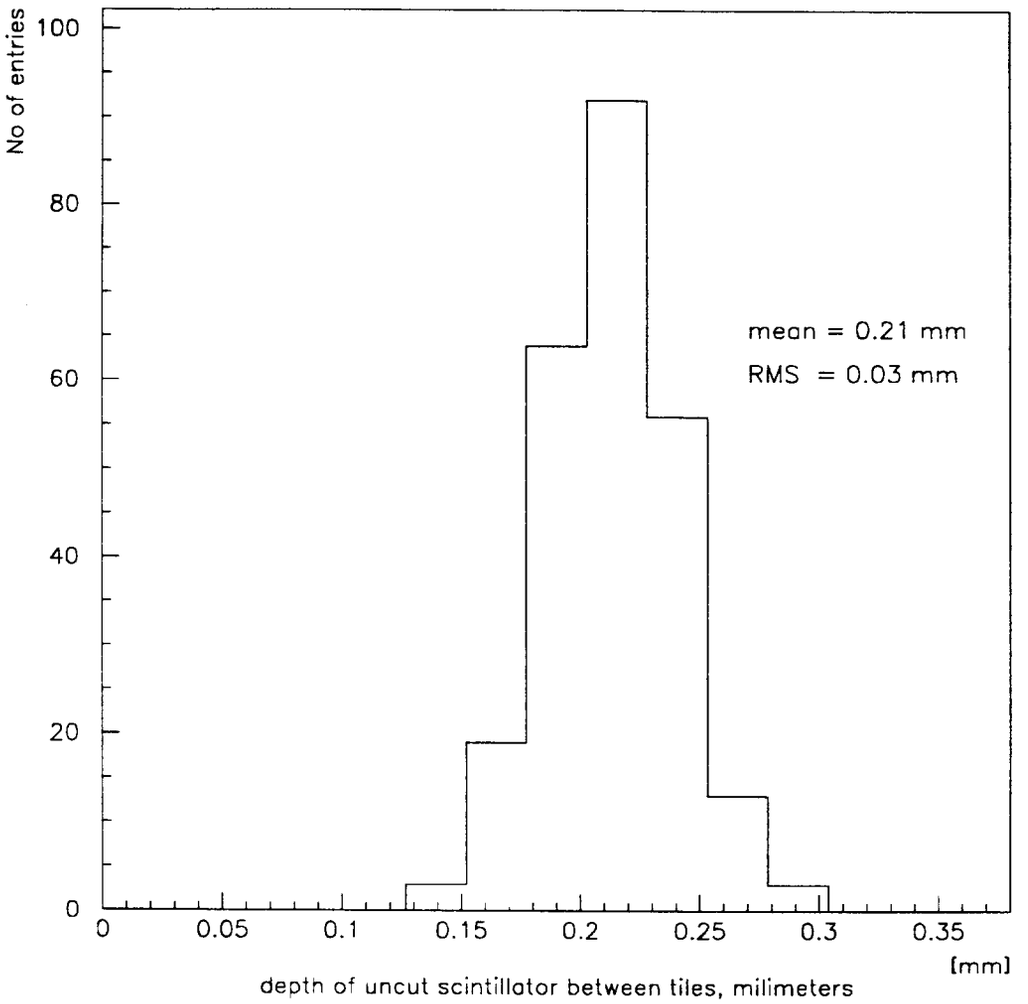

Fig. 31. The distribution of the thickness of uncut material below the separation grooves between neighboring tiles. The sample of megatiles used in this measurement corresponds to the scintillator plates used in the production of L17 and L18 megatiles.

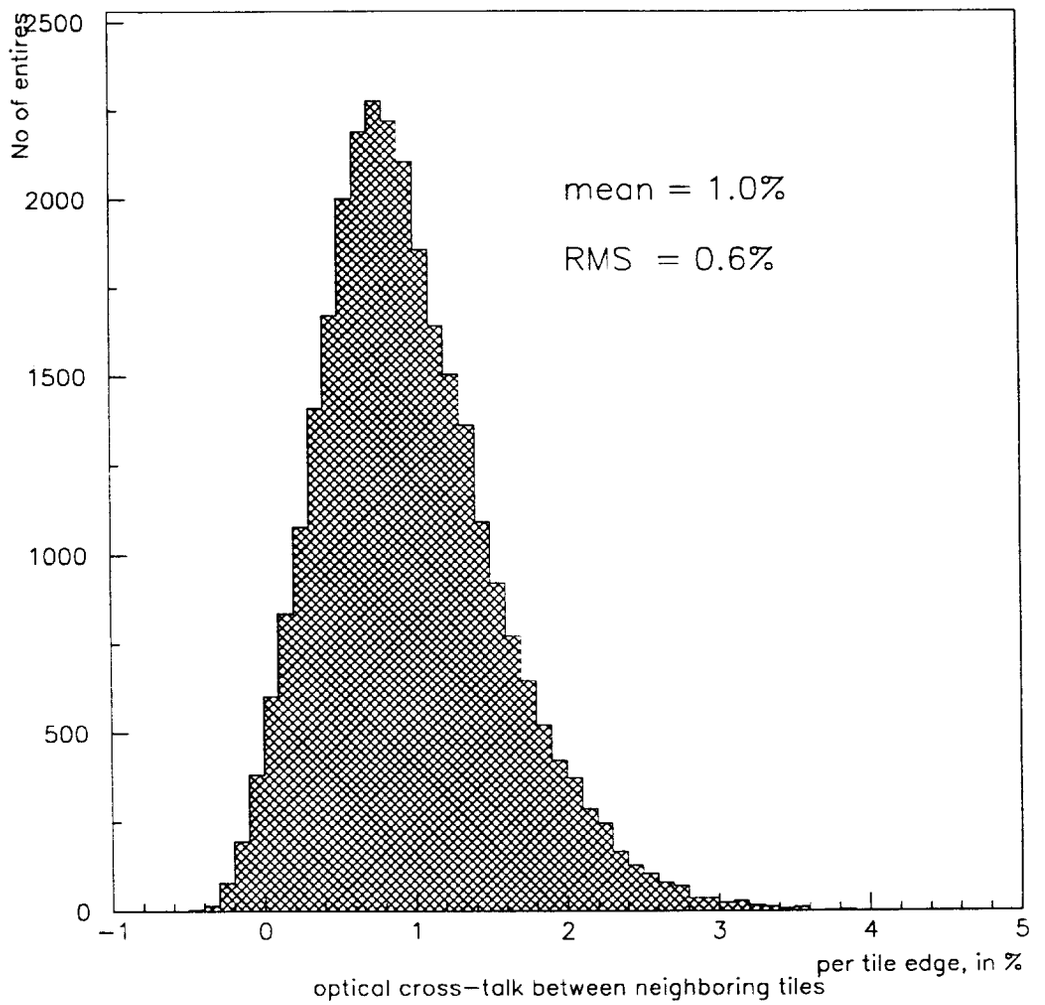

Fig. 32. The distribution of the optical cross-talk between the neighboring tiles, as measured during QC tests of Hadron megatiles. The data has been corrected for the radiation cross-talk due to the finite size of the lead cone used to collimate the γ source. The data in the plot does not include the two highest η tiles (tiles 1 and 2, as depicted on Fig. 3). For these tiles, due to their small transverse size, the uncertainty in the correction due to radiation cross-talk was too large to precisely determine the optical cross-talk.